The virtual brain endocast of *Trogosus* (Mammalia, Tillodontia) and its relevance in understanding the extinction of archaic placental mammals

Short running page heading: Virtual brain endocast of *Trogosus*

Ornella C. Bertrand[1,2*], Marina Jiménez Lao[2], Sarah L. Shelley[2,3], John R. Wible[3], Thomas E. Williamson[4], Meng Jin[5], and Stephen L., Brusatte[2,4]

*Corresponding author

[1]Institut Català de Paleontologia Miquel Crusafont, Universitat Autònoma de Barcelona, Edifici ICTA-ICP, c/ Columnes s/n, Campus de la UAB, 08193 Cerdanyola del Vallès (Barcelona), Spain

[2]School of GeoSciences, University of Edinburgh, Grant Institute, Edinburgh, Scotland, UK

[3]Section of Mammals, Carnegie Museum of Natural History, 15213, Pittsburgh, PA, USA

[4]New Mexico Museum of Natural History and Science, 87104, Albuquerque, NM, USA

[5]Division of Paleontology, American Museum of Natural History, 10024, New York, NY, USA

Abstract – After successfully diversifying during the Paleocene, the descendants of the first wave of mammals that survived the end-Cretaceous mass extinction waned throughout the Eocene. Competition with modern crown clades and intense climate fluctuations may have been part of the factors leading to the extinction of these archaic groups. Why these taxa went extinct has rarely been studied from the perspective of the nervous system. Here, we describe the first virtual endocasts for the archaic order Tillodontia. Three species from the middle Eocene of North America were analyzed: *Trogosus hillsii, Tr. grangeri*, and *Tr. castoridens.* We made morphological comparisons with the plaster endocast of another tillodont, *Tillodon fodiens*, as well as groups potentially related to Tillodontia: Pantodonta, Arctocyonidae, and Cimolesta. *Trogosus* shows very little inter-specific variation with the only potential difference being related to the fusion of the optic canal and sphenorbital fissure. Many ancestral features are displayed by *Trogosus*, including an exposed midbrain, small neocortex, orbitotemporal canal ventral to rhinal fissure, and a broad circular fissure. Potential characters that could unite Tillodontia with Pantodonta, and Arctocyonidae are the posterior position of cranial nerve V_3 exit in relation to the cerebrum and the low degree of development of the subarcuate fossa. The presence of large olfactory bulbs and a relatively small neocortex are consistent with a terrestrial lifestyle. A relatively small neocortex may have put *Trogosus* at risk when competing with artiodactyls for potentially similar resources and avoiding predation from archaic carnivorans, both of which are known to have had larger relative brain and neocortex sizes in the Eocene. These factors may have possibly exacerbated the extinction of Tillodontia, which showed highly specialized morphologies despite the increase in climate fluctuations throughout the Eocene, before disappearing during the middle Eocene.

Keywords: Eocene, neocortex, olfactory bulb, ecology, environment, senses, behavior, competition

Introduction

Sixty-six million years ago, the end-Cretaceous mass extinction led to the collapse of ecosystems on land, in the air, and in the sea. Mammals survived and recovered relatively rapidly, with the appearance of a plethora of new species of placentals and close relatives during the Paleocene (Rose, 2006). Many of these species are considered archaic placentals, as they have been challenging to place in the tree of life because of their unusual morphology compared to modern groups that we know today as crown clades and which include for example artiodactyls, perissodactyls, carnivorans, rodents, euprimates, and bats (Rose, 2006). Remnants of the descendants of this first wave of archaic placental mammals remained throughout the Eocene, when crown clades started diversifying. However, the archaic lineages began to decrease in diversity and by the end of the Eocene, most of them were extinct. The reason for their extinction remains contentious, but a prevalent hypothesis holds that they may have been outcompeted by the crown clades (Lucas and Schoch, 1998). More recently, new evidence relying on the study of the neurosensory system has reached similar conclusions. Crown clades had higher relative brain and neocortical sizes translating into an increase in behavioural flexibility compared to archaic species, which may have given a selective advantage to the former (Bertrand et al., 2022). However, more information on the detailed neurosensory anatomy of archaic placentals is necessary to better understand the possible link between their brains and their extinction. Here, we focus on one particular genus belonging to the archaic order, Tillodontia, and describe its brain anatomy for the first time using virtual endocasts.

Tillodonts first appear in the fossil record in the early Paleocene of Asia, which suggest that they originated and radiated from this part of the world (Rose, 2006, Rose et al., 2009). Material has also been recovered from North America (early Paleocene to middle Eocene) and

Europe (early Eocene). Recently, tillodont teeth have also been found in the early Eocene of India (Rose et al., 2009, 2013). These various occurrences strongly suggest faunal exchange between the different landmasses. The last tillodonts are found in North America and Asia during the middle Eocene (Lucas and Schoch, 1998, Rose et al., 2009). Tillodonts had a relatively specialized morphology and a rather low taxonomic diversity (~15 species). They are characterized by hypertrophied gliriform incisors with restricted enamel. Additionally, the second pair of incisors is enlarged and in younger species, these teeth are ever-growing and hypsodont (Gazin, 1953, Rose, 2006). Postcranial remains suggest that the earliest tillodonts were terrestrial and may have been able to climb (e.g., esthonychines; Rose, 2001), while more derived members such as trogosines were specialized in digging behavior and used their moderately large and recurved claws to unearth roots and tubers (Gingerich and Gunnell, 1979).

The interordinal phylogenetic relationships of Tillodonta are still an open question and two main hypotheses have been proposed. They may have been closely related to arctocyonid 'condylarths' (Gazin, 1953, Szalay, 1977), or part of the larger group Cimolesta, within which they would have been closely related to pantodonts (McKenna and Bell, 1997, Rose, 2006). The relationship between pantodonts and tillodonts is supported by a uniquely shared feature: dilambdodont dentition (Chow and Wang, 1979, Gingerich and Gunnell, 1979, Lucas, 1993). Moreover, based on a study of a large number of morphological characters, pantodonts and tillodonts were found closely related in a recent higher-level phylogenetic analysis of mammals (Muizon et al., 2015). Tillodonts are all placed in one family Esthonychidae, subdivided into two subfamilies mainly based on the morphology of the second incisors. Esthonychinae is the more generalized subfamily and includes two genera (Gingerich and Gunnell, 1979), while Trogosinae

is composed of five genera and displays a more specialized morphology including rootless second incisors (Gazin, 1953).

One aspect of tillodont evolution that remains particularly understudied is their neurosensory system. The only brain endocast ever studied for this group is a physical endocast of *Tillodon fodiens.* A simple reconstruction and very brief description of the cast was first published by Marsh (1876: fig. 1). Later, Edinger (1929: fig. 119b, c) produced more detailed illustrations of the cast with a more detailed but still brief description, as she did not have the cranium at her disposal. Gazin reused Edinger's drawings, added a ventral view of the cast and made a more detailed description of the cast. Unfortunately, the cast made for this specimen was not of high-quality and displayed for example an unexpectedly dorsally enlarged cerebellum in which hardly any structures were identifiable (see Gazin, 1953: fig. 20b). This would suggest the possible presence of large canals for vessels that would have collapsed, leading to a larger endocranial cavity. The low number of studies on the brain evolution of Tillodontia is not an anomaly. Before CT scanning technology became widely accessible, very little work had focused even on groups for which high quality skull fossils are available. Generating brain endocasts for extinct species required destructive techniques such as making cross-sectioned slices of the actual specimens and peeling the cranium to access the imprint of the brain (e.g., Novacek, 1986, Meng et al., 2003). Another method, only possible in crania without sediment inside, consisted of filling the endocranial cavity with latex, which can be removed once solidified (Russell and Sigogneau, 1965).

With the use of CT data to virtually extract brain endocasts, studies describing the brain evolution of mammals and other vertebrates have flourished over the past two decades (Dozo et al., 2023). In particular, a growing body of literature on Eocene crown placental mammals such

as rodents (Bertrand et al., 2016, 2019), euprimates (Kirk et al., 2014, Ramdarshan and Orliac, 2016, Harrington et al., 2016, 2020), artiodactyls (Orliac and Gilissen, 2012), afrotherians (Benoit et al., 2013), and chiropterans (Maugoust and Orliac, 2021) has been published. However, very few virtual endocasts of archaic Eocene mammals have been described; these include plesiadapiforms (Silcox et al., 2009, 2010), the 'condylarth' *Hyopsodus* (Orliac et al., 2012), the anagalid *Anagale* (López-Torres et al., 2023), and notoungulates (Perini et al., 2022). Descriptions of virtual endocasts from Paleocene archaic mammals are also rare; these include *Labidolemur* (Silcox et al., 2011), the plesiadapiforms *Plesiadapis* and *Niptomomys* (Orliac et al., 2014, White et al., 2023), the pantodont *Alcidedorbignya* (Muizon et al., 2015), the 'condylarth' *Carsioptychus* (Cameron et al., 2019), the taeniodont *Onychodectes* (Napoli et al., 2018), and the 'condylarth' *Chriacus* (Bertrand et al., 2020). Finally, a large number of archaic mammals were virtually segmented by the study from Bertrand et al. (2022), but many of these brain endocasts have yet to be described in detail.

Here, we describe the first virtual endocasts of a tillodont, belonging to the middle Eocene *Trogosus*. This genus is well-known from North American localities in Wyoming and Colorado, but remains have also been found in California, Utah, and British Columbia (Gazin, 1953, Robinson, 1966, Miyata, 2007b, Miyata and Deméré, 2016) and Japan (Miyata, 2007a). The phylogenetic relationships among the species within the genus *Trogosus* are not resolved. Several authors have suggested that the sympatric species *Tr. castoridens* and *Tr. hyracoides* from the Green River Basin in Wyoming could be synonymous (Robinson, 1966, Lucas and Schoch, 1998) and rostrum length disparity between both taxa might be related to sexual dimorphism (Gazin, 1953). A similar hypothesis was proposed for another sympatric pair, *Tr. hillsii* and *Tr. grangeri* from the Huerfano Basin in Colorado, also displaying a difference in the

length of the rostrum. More recently, Miyata and Deméré (2016) described a new specimen from the Delmar Formation (San Diego, California) that they attributed to *Tr. castoridens*. They also generated a new phylogenetic analysis including this specimen and new cranio-dental and postcranial elements. Miyata and Deméré (2016) found similar groupings (i.e., sister taxon pairs of *Tr. hillsii* + *Tr. grangeri* and *Tr. castoridens* + *Tr. hyracoides*) but maintained the four taxa as separate species based on cranial differences. They hypothesized that the shortening of the rostrum may have evolved convergently in *Tr. hillsii* and *Tr. castoridens*. Ultimately, a consensus has been difficult to reach because of the small sample size and the fragmentary nature of most *Trogosus* fossils. Study of the neurosensory system of *Trogosus*, one of the most derived tillodont genera, may provide new insight into the unresolved phylogenetic relationships of Tillodontia, and raise hypotheses for whether, and how, neurosensory systems may have been related to their eventual extinction.

Institutional abbreviations

AMNH, American Museum of Natural History, New York, NY, USA; CR, Cernay Les Reims, France; CRL, Conglomérat de Cernay of Lemoine collection and quarry of Mont de Berru, Paris, France; MCZ, Museum of Comparative Zoology, Cambridge, MA, USA; MHNC, Museo de Historia Natural 'Alcide d'Orbigny', Cochabamba, Bolivia; MNHN, Muséum Nationale d'Histoire Naturelle, Paris, France; SDSM, South Dakota School of Mines, SD, USA; SDSNH, San Diego Natural History Museum, San Diego, California, USA.; UM, University of Michigan, Michigan, USA; USNM, United States National Museum of Natural History, Washington, D.C., USA; YPM, Peabody Museum of Natural History, Yale University, New Haven, Connecticut, USA.

Materials and methods

This study includes skulls of three different species belonging to the genus *Trogosus*: *Tr. hillsii*, *Tr. grangeri*, and *Tr. castoridens* that are all from the middle Eocene. The skulls of *Tr. hillsii* and *Tr. grangeri* were both described by Gazin (1953) and these two specimens are the types of both species. The majority of the skull is preserved in *Tr. hillsii* (USNM 17157) but lacks parts of the rostrum and is from the upper Huerfano B (Huerfano Basin, Colorado; no details on the site). *Trogosus grangeri* (AMNH 17008) includes a complete skull and some postcranial elements. It is also from Huerfano B (Huerfano-Muddy divide, 3 miles west of Gardner, Huerfano Basin, Colorado). Photographs of both crania were published by Miyata and Deméré (2016). *Trogosus castoridens* was first described by Leidy in 1871 based on a partial mandible with left and right dentaries and incomplete dentition (illustrated in Gazin, 1953), which was the only material known for the species until a new specimen was described by Miyata and Deméré (2016). *Trogosus castoridens* (SDSNH 40819) is a nearly complete cranium with an almost complete dentition and some postcranial elements (Miyata and Deméré, 2016). This specimen is from the upper portion of the Delmar Formation (San Diego County, California).

Comparative sample

We compared *Trogosus* brain endocasts with potentially closely related groups. As a framework, we considered the phylogenetic analysis of Muizon et al. (2015), which placed Tillodontia within Laurasiatheria as part of a cluster of early placental mammals, and not particularly closely related to any crown clades in the most parsimonious trees from their analyses. Instead, Tillodontia was placed close to the archaic groups Pantodonta and

Arctocyonidae (Muizon et al., 2015: figs. 121, 122). However, the tree topologies are relatively unstable due to the presence of a high-level of homoplasy and these results should be interpreted with caution (Muizon et al., 2015). We made comparisons with the tillodont *Tillodon fodiens* (YPM 11087; Gazin, 1953), the pantodont *Alcidedorbignya inopinata* (MHNC 8372; Muizon et al., 2015), the arctocyonid 'condylarths' *Chriacus baldwini* (MCZ 20676; Bertrand et al., 2020), *Arctocyon primaevus* (MNHN CR 700), and *Arctocyonides arenae* (MNHN CR 733; Russell and Sigogneau, 1965), the 'condylarth' *Hyopsodus lepidus* (AMNH 143783; Orliac et al., 2012), the 'condylarth' *Pleuraspidotherium aumonieri* (MNHN CRL 252; Russell and Sigogneau, 1965), and the periptychid 'condylarth' *Carsioptychus coarctatus* (AMNH 27601; Cameron et al., 2019). Because of possible close relationships with the eutherian, and possibly basal placental, mammal group Cimolesta (Rose, 2006), we compared *Trogosus* with the taeniodont *Onychodectes tisonensis* (AMNH 785; Napoli et al., 2018), the leptictid *Leptictis* (AMNH FM 96730; Novacek, 1982, 1986), and the palaeoryctid *Eoryctes melanus* (UM 68074; Thewissen and Gingerich, 1989, Wible, 2022). For natural or handmade endocasts, we only used well-described and illustrated specimens. Therefore, we did not make comparisons with drawn endocasts from the publications of Cope (1877), Marsh (1876), and Schoch (1983).

Virtual endocast acquisition

Two of the three specimens were CT scanned for this project: *Tr. grangeri* (AMNH FM 17008) was scanned at the Microscopy and Imagery Facility (MIF) at the AMNH and *Tr. hillsii* (USNM 17157) was scanned at the University of Texas, in the High-Resolution X-Ray CT Facility (UTST). They were scanned at a resolution (voxel size), respectively, of 0.08918041 mm and 0.145 mm. The specimen of *Tr. castoridens* (SDSNH 40819) was kindly shared with us by K. Miyata and T. Deméré. The voxel size for this specimen is 0.1 mm. This specimen was

scanned by K. Miyata using a High-Resolution X-Ray CT scanner, TXS320-ACTIS (TESCO Co., Yokohama, Japan), at the Fukui Prefectural Dinosaur Museum.

The three specimens were segmented in Avizo® 9.7.0 software (Visualization Sciences Group, 1995-2019). New labelfield modules were created to segment the endocranial cavity of each specimen in order to visualize the brain endocast separately from the cranium. The pen tool was used during the segmentation process because of the low contrast between the density of the bone and the endocranial cavity that was filled with matrix. *Trogosus castoridens* (SDSNH 40819) was the most challenging to segment because the density of the bone and the matrix contained inside the endocranial cavity were very similar. In certain regions, the bone was not preserved, and a straight line was used to link the two nearest pieces of bone. We followed Bertrand et al. (2020), for the brain endocranial anatomical descriptions. For the cranial vascular system description, we followed Muizon et al. (2015) and Wible (2022). A surface rendering was generated for the three virtual endocasts using unconstrained smoothing. To estimate the volume of the endocast, the module 'generate surface' was used directly onto the labelfield module of *Tr. hillsii* (USNM 17157). Originally, we reconstructed the olfactory bulbs in *Tr. grangeri* (AMNH FM 17008) and included them in the measurement dataset of Bertrand et al. (2022). We re-checked the CT data and were not confident in the original reconstruction; the cribriform plate surrounding the olfactory bulbs could not be identified with certainty because of limited preservation and low contrast of the CT scan. Because of this uncertainty, we decided not to report the endocranial volume for *Tr. grangeri* (AMNH FM 17008). The virtual brain endocast of *Tr. castoridens* (SDSNH 40819) appears crushed dorsoventrally, and therefore no volumetric measurements were performed on this specimen.

Palaeobiological calculations

Body mass estimation – We used dental measurements to determine the body mass of *Tr. hillsii* (USNM 17157) using data reported by Miyata (2007a) for this specimen. The body masses for *Tr. grangeri* (AMNH FM 17008) and *Tr. castoridens* (SDSNH 40819) were not estimated because the brain endocasts were too incomplete for providing an accurate brain endocranial volume. We used the following dental equations to estimate the body mass of *Tr. hillsii* (USNM 17157): the 'All mammal curve' M_1 area equation from Legendre (1989), and the 'non selenodont taxa' M_1 length and area equations from Damuth (1990). The equations and body mass estimates are presented in Table 1. We used the three values for our quantifications below to take into account the uncertainty of the body mass. Because the cranium of *Tr. hillsii* (USNM 17157) is incomplete rostrally, skull length could not be used to determined body mass. We could not use postcranial elements to determine body mass of *Tr. hillsii* (USNM 17157). An almost complete humerus AMNH 17011 from the Huerfano has been attributed to the genus *Trogosus*, but cannot be attributed to a species (Gazin, 1953: fig. 29; Miyata, 2007b) and therefore would not represent a good candidate. Femora have been recovered for *Tr. hillsii*, but linear measurements for these bones have not been generated yet (Gazin, 1953: fig. 35).

Neurobiology – Linear measurements of the three virtual brain endocasts were taken and ratios of these dimensions were generated following Bertrand and Silcox (2016; Table 2). The olfactory bulb volume for *Tr. hillsii* (USNM 17157) was estimated using the module 'volume edit' tool in Avizo® 9.7.0 software (Visualization Sciences Group, 1995-2019). For *Tr. grangeri* (AMNH 17008), the value is not reported here because of poor preservation that may bias an accurate measurement. We also want to avoid overestimation of the volume of these structures and of the overall endocranial volume. The volume was also not generated for *Tr. castoridens* (SDSNH 40819) because of poor preservation. The neocortical surface area of *Tr. hillsii* (USNM

17157) was quantified by virtually isolating it from the rest of the brain endocast using the pen tool in Avizo® 9.7.0 software (Visualization Sciences Group, 1995-2019). The surface of the neocortex was not estimated in *Tr. grangeri* (AMNH 17008) and *Tr. castoridens* (SDSNH 40819) because the boundaries of the neocortex were hardly distinguishable.

Statistical analyses – We performed a series of statistical analyses on middle Eocene taxa (Bertrand et al., 2023, table S1). The age of each specimen was based on the locality where the specimen was found or on the species age when the locality was unknown. Brain endocasts of species for which the age could not be attributed to a single epoch subdivision was categorized using the oldest subdivision (e.g., middle to late Eocene was categorized as middle Eocene). For more information about the exact age in millions of years of the specimens, see Bertrand et al. (2022: table S19). The decision not to include early and late Eocene taxa is based on the presence of a temporal effect on brain size in mammals (Jerison, 1973, Bertrand et al., 2022), which could lead to misleading interpretations. Indeed, there is a clear increase in relative brain size from the Paleocene to the present, which occurred independently in different mammalian lineages (Jerison, 1961, Bertrand et al., 2022). We investigated the relationship between the 1) brain volume and body mass, 2) olfactory bulb volume and brain volume, 3) olfactory bulb volume and body mass, and 4) neocortical surface area and brain surface area. We elected to perform an OLS regression without taking the effect of phylogeny into account because of the uncertainty of the relationships among archaic and crown taxa, and among the three tillodonts themselves. Additionally, the sensitivity analyses performed in Bertrand et al. (2022) showed that phylogeny did not have an impact on the reults. We plotted the size of the olfactory bulbs against the endocranial volume to compare the proportional differences in the olfactory bulbs and

neocortical sizes. The olfactory bulbs were plotted against body mass to estimate the actual size variation of these structures.

All analyses were performed in R v3.6.2 (R Core Team, 2019) and R studio v2022.07.2 (R Studio Team, 2022). For the OLS linear regressions, we used the function "ggplot" in the package *ggplot2* (Wickham, 2016) for visualization and the function "gls" in the package *nlme* (Pinheiro et al., 2018) to create three regression lines for the four endocranial relationships: 1) all taxa, 2) archaic taxa, and 3) crown clades (Bertrand et al., 2023, table S2). We generated the residuals for all taxa (1) using the function "residuals" in the package *stats* (Chambers and Hastie, 1992; see Bertrand et al., 2023, table S3). Then, we produced boxplots of these residuals to compare individual crown clades and archaic taxa with *Tr. hillsii* using the function "ggboxplot" in the package *ggplot2* (Wickham, 2016). Normality of the data was assessed using a Shapiro-Wilk test (data normally distributed: p-value > 0.05). Then homogeneity of the variances (equality of the variance: p-value > 0.05) was verified using a Levene's test (data not normally distributed) or Bartlett's test (data normally distributed). When the variances were equal, we used Fisher-Pitman Permutation tests with the functions "oneway-test" in the package *coin* (Hothorn et al., 2006) and "pairwisePermutationTest" in the package *rcompanion* (Mangiafico, 2017). Otherwise, we used the Welch test (Welch, 1951) and the functions "welch.test" and "paircomp" in the package *onewaytests* (Dag et al., 2018). These tests allowed us to assess whether groups had significant differences in endocranial residuals but were only performed with more than two individuals per categories (Bertrand et al., 2023, table S4). Additionally, we performed ANOVAs on the four endocranial relationships to evaluate the difference in slope and intercept between crown clades and archaic taxa (Bertrand et al., 2023, table S5).

Finally, the data were also organized by dietary groups: herbivores and carnivores-omnivores for the ungulate and carnivoran species only based on the morphology of their teeth and previous work (Bertrand et al., 2023, table S1). In these analyses, we also made the distinction between Eocene archaic taxa and crown clades. We analyzed the endocranial residuals (Bertrand et al., 2023, table S6) using this classification to investigate whether there was any significant difference in the neurosensory variables between dietary guilds. We visualized these analyses using the function "ggplot" in the package *ggplot2* (Wickham, 2016). Permutation tests were also conducted for this set of analyses using similar methods as described above (Bertrand et al., 2023, table S7).

We produced encephalization quotient values and residuals from the OLS linear regression between brain volume and body mass of our middle Eocene sample (Bertrand et al., 2023, table S2). The encephalization quotient (EQ) was first proposed by Jerison (1973; Ei / Ec) and corresponds to the ratio between the actual brain size (Ei) of a given species (i) and the brain size expected for a hypothetical 'typical' mammal of the same body mass (Ec; Martin, 1990). Here, we generated our own EQ equation based on the OLS regression for our sample of middle Eocene taxa (see EQ values in Bertrand et al., 2023, table S3). We elected to not use the equations from Jerison (1973) or Eisenberg (1981) to generate EQ values because of biases due to the sample size used to generate these EQ equations.

Descriptions and comparisons

The brain endocast of *Tr. hillsii* is complete (Figs. 1, 2A, D and 3A, B) with a brain volume of 61021.2 mm^3 (Table 2). The brain endocast of *Tr. grangeri* (Figs. 2B, E and 3C, D) is relatively complete; however fewer details of the anatomy are visible. *Trogosus castoridens*

(SDSNH 40819; Figs. 2C, F and 3E, F) is flattened dorsoventrally compared to the two other specimens; however, the cranium appears undeformed (See Miyata and Deméré, 2016). Possible endocranial deformation may have occurred as the bone appears very thick in the cross-section of the CT data (Bertrand et al., 2023, fig. S1).

Olfactory bulbs – The olfactory bulbs are well preserved in *Tr. hillsii*. In dorsal view, the posterior width of the olfactory bulbs is wider than the anterior width. The bulbs are also medially separated by an antero-posterior gap (Fig. 2A). Although, not complete, the gap is visible at the base of the olfactory bulbs in *Tr. grangeri*, which suggests a similar olfactory bulb morphology (Fig. 2B). *Leptictis* also displays a wider posterior width for the olfactory bulbs, but no gap in between (Novacek, 1986: fig. 30). Similar to *Trogosus, Al. inopinata* has a gap running medially along the olfactory bulbs, but their shape is more ovoid (Fig. 5D). The bulbs are ovoid and conjoined in *H. lepidus* (Fig. 5C). In *Ar. primaevus*, there is a small gap between both bulbs anteriorly; however, their shape is difficult to describe because of limited preservation (Russell and Sigogneau, 1965). Still in dorsal view, the olfactory bulbs appear to be ovoid in *Ch. baldwini, O. tisonensis* (Fig. 6A, B), *Ca. coarctus* (Cameron et al., 2019: fig. 3c), and *Ad. arenae* (Russell and Sigogneau, 1965). It is not possible to comment on the condition in *Ti. fodiens, Pleuraspidotherium,* and *E. melanus* because of lack of preservation. The olfactory bulbs are positioned posteriorly to the molars in *Tr. hillsii* (Fig. 1C), which is similar to the condition observed in *O. tisonensis* (Napoli et al., 2018: fig. 1a), *Ch. baldwini* (Bertrand et al., 2020: fig. 3b), and *Ca. coarctatus* (Cameron et al., 2019: fig. 2d). The olfactory bulbs are positioned above the teeth in *H. lepidus* (Orliac et al., 2012: fig. 2a). This condition can only be determined while visualizing the endocast and the translucent cranium together. Therefore, it could not be determined for *Ti. fodiens, Al. inopinata, Leptictis, Ar. primaevus, Ad. arenae,*

Pleuraspidotherium, and *E. melanus*. The circular fissure separates the olfactory bulbs from the cerebrum and is greatly expanded in *Tr. hillsii* (Figs. 2A, 3A) and *Tr. grangeri* (Fig. 2B, 3C). A similar pattern is visible in the Paleocene taxa *Ch. baldwini*, *Al. inopinata*, *O. tisonensis* (Fig. 5), *Ar. primaevus,* and *Ad. arenae* (Russell and Sigogneau, 1965). In dorsal view, the circular fissure appears narrower in *Leptictis* (Novacek, 1986: fig. 30) and *E. melanus* (Thewissen and Gingerich, 1989: fig. 7). The condition is not clear in *Ti. fodiens, H. lepidus*, *Ca. coarctatus*, and *Pleuraspidotherium.*

Cerebrum and midbrain – In dorsal view, the cerebrum has an ovoid shape anteriorly and lacks the preservation of the superior sagittal sulcus defining both hemispheres antero-medially in the well-preserved *Tr. hillsi* (Fig. 2A). This pattern is unlikely to be due to preservation; however, it cannot be ruled out for the two other *Trogosus* specimens because they are well less preserved (Figs. 2B, 2C). In contrast, the cerebral hemispheres have a straight outline anteriorly in *Leptictis* (Novacek, 1986: fig. 30) and *E. melanus* (Thewissen and Gingerich, 1989: fig. 7). This feature cannot be identified for other taxa because of lack of preservation. The cerebral hemispheres are interrupted medially by the superior sagittal sulcus running between the frontal lobes of the neocortex in *Al. inopinata, Ch. baldwini, H. lepidus* (Fig. 5)*, Ar. primaevus, Ad. arenae* (Russell and Sigogneau, 1965)*, Leptictis* (Novacek, 1986: fig. 30), and *E. melanus* (Thewissen and Gingerich, 1989: fig. 7). Because of preservation, this feature is not easily identifiable in *Ti. fodiens, O. tisonensis, Ca. coarctatus*, and *Pleuraspidotherium*. *Trogosus* appears to have had a completely lissencephalic brain (Figs. 2A-C) similar to *H. lepidus* (Fig. 5C). Possible sulci have been identified in *Ar. primaevus, Ad. arenae* (Russell and Sigogneau, 1965)*, Al. inopinata* (Muizon et al., 2015: fig. 54), *Leptictis* (Novacek, 1986: fig. 30), *E. melanus* (Thewissen and Gingerich, 1989: fig. 7), and *O. tisonensis* (Napoli et al., 2018: fig. 2). Because

of preservation, we cannot verify the presence of sulci in *Ti. fodiens, Ch. baldwini, Ca. coarctatus*, and *Pleuraspidotherium*.

The cerebrum is composed of two regions in mammals known as the neocortex and the paleocortex (= piriform lobe). The separation between both structures corresponds to the rhinal fissure (Martin, 1990). This key landmark can be used to provide information on the degree of expansion of the neocortex (Jerison, 2012, Long et al., 2015). The rhinal fissure is visible dorsally in mammals with less expanded neocortices or laterally in taxa with more expansive neocortices. In Euarchontoglires, there is an overlap between the rhinal fissure and the orbitotemporal canal (e.g., Martin, 1990, Silcox et al., 2010, Bertrand and Silcox, 2016). However, this relationship is not consistent across Mammalia, and in some groups, the rhinal fissure may occupy a more dorsal position compared to the orbitotemporal canal due to a lesser expansion of the neocortex. Furthermore, the ramus supraorbitalis of the stapedial artery (Wible, 1987) may not always be enclosed inside an orbitotemporal canal, as observed in the anagalid *Anagale gobiensis* (AMNH 26079; López-Torres et al., 2023) where no canal could be identified. The orbitotemporal canal is preserved and visible in *Tr. hillsii* and it overlaps with the rhinal fissure posteriorly but then runs ventrally from the latter anteriorly. After separating from the course of the orbitotemporal canal, the rhinal fissure slopes up and points to the direction of the dorsal aspect of the olfactory bulbs (Fig. 3A). Both structures are challenging to identify in *Tr. castoridens* and *Tr. grangeri* because of poor preservation of the area (Fig. 3C-F). The orbitotemporal canal runs ventrally to the rhinal fissure in *Al. inopinata*, *Ch. baldwini* (Fig. 5 I, L)*, Pleuraspidotherium, Ar. primaevus,* and *Ad. arenae* (Russell and Sigogneau, 1965). The rhinal fissure and the orbitotemporal canal have been described as running together anteriorly in *Leptictis* (Novacek, 1982) and *E. melanus* (Thewissen and Gingerich, 1989). The orbitotemporal

canal is not visible in *H. lepidus*. The relationship between these two structures cannot be reliably identified in *Ti. fodiens, O. tisonensis,* and *Ca. coarctatus*.

In the dorsal view of *Tr. hillsii*, the midbrain is identified as a small patch with boundaries challenging to trace and without clearly defined colliculi (Fig. 2A). The lack of good preservation of this region in *Tr. grangeri* and *Tr. castoridens* does not allow us to confidently identify this structure in these two specimens. A similar condition is observed in *Al. inopinata*, *H. lepidus* (Fig. 5C, D)*, E. melanus* (Thewissen and Gingerich, 1989: fig. 7)*, Pleuraspidotherium, Ar. primaevus,* and *Ad. arenae* (Russell and Sigogneau, 1965) in which the midbrain is exposed and not covered by the cerebrum. In contrast to other taxa, *E. melanus* displays a more complex midbrain with the presence of caudal colliculi (Thewissen and Gingerich, 1989: fig. 7). The midbrain was described as not being exposed in *Leptictis* (Novacek, 1982, 1986). This condition cannot be identified in *Ti. fodiens, Ch. baldwini, O. tisonensis,* and *Ca. coarctatus* because of lack of preservation.

Cerebellum – The cerebellum of *Tr. hillsii* is complete but detailed structures, including the boundaries between the vermis and the lobes of the cerebellum, are hard to identify (Fig. 2A). The width of the cerebellum and cerebrum are similar in dorsal view for the three *Trogosus* specimens (Table 2; Fig. 2A-C) as well as in *Ti. fodiens*. In contrast, the cerebellum appears narrower in *Ch. baldwini*, *Al. inopinata*, *H. lepidus* (Fig. 5 A, C, D), *Leptictis* (Novacek, 1986: fig. 30), *E. melanus* (Thewissen and Gingerich, 1989: fig. 7)*,* and *Ca. coarctatus* (Cameron et al., 2019: fig. 3c). The remaining specimens are not complete enough to make comparisons (i.e., *O. tisonensis, Pleuraspidotherium, Ar. primaevus,* and *Ad. arenae*).

The petrosal lobules, as defined in previous studies as regions of the cerebellum filling the subarcuate fossa (e.g., Bertrand et al., 2020, Lang et al., 2022), are very subtle in *Tr. hillsii*,

and this is unlikely due to poor preservation of the area (Fig. 2A). The two other specimens, *Tr. grangeri* and *Tr. castoridens*, display even fewer details of the anatomy of the cerebellum (Fig. 2B, C). *Trogosus* may have a subarcuate fossa where the petrosal lobules are usually present such as in rodents (Bertrand et al., 2017), but because we could not reconstruct the semicircular canals of the inner ear, the petrosal lobules could not be correctly identified. In any case, the subarcuate fossa of *Trogosus* would have not been very deep and similar to *Al. inopinata* (Muizon et al., 2015: fig. 54a), and *Pantolambda bathmodon* (NMMNHS 14538; isolated petrosal), which has a very small petrosal lobule volume (0.01%; Bertrand et al., 2022). Muizon et al. (2015) also mentioned the tillodont *Azygonyx* (CT data of UM 68511) as not having a large subarcuate fossa. However, we could not access the CT data of this taxon to see how similar the condition was to *Trogosus*. The petrosal lobules are also very small in *O. tisonensis* (0.06%; Fig. 5J) and in *Ar. primaevus* (0.13%; IRSNB M 2332). They are slightly larger in *Ch. baldwini* (0.26%; Fig. 5I) and *H. Lepidus* (0.24%; Fig. 5G). They are larger in *Pleuraspidotherium aumonieri* (0.53%; UCMP 61488) and *Leptictis* sp. (1.63%; SDSM 62369; AMNH 62369 in Bertrand et al., 2022). The quantitative measurements are from Bertrand et al. (2022). The petrosal lobules could not be identified in *Ti. fodiens* and were not estimated in *Ad. arenae, Ca. coarctatus*, and *E. melanus*.

Cranial nerves and blood vessels – On the ventral surface of the endocast, the casts for some cranial nerves and vessels can be distinguished. The canals for the optic nerves (cranial nerve II) are positioned below the posterior aspect of the circular fissure in *Tr. hillsii* (Figs. 2D, 3A). In the natural endocast of *Ti. fodiens* (Gazin, 1953: fig. 20), the optic nerve canals and the sphenorbital fissure both hold a similar position to *Tr. hillsii* (Fig. 6B). In contrast, only one foramen and canal are present on each side in *Tr. grangeri* (Figs. 2E, 3D) and in *Tr. castoridens* (Figs. 2F, 3F), which would suggest that the optic nerve and content of the sphenorbital fissure

exited through a common foramen in these two taxa. All compared taxa have an optic foramen and canal separated from the sphenorbital fissure (Fig. 5). The ancestral condition for eutherians and placental mammals corresponds to having the ophthalmic veins and cranial nerves III (oculomotor), IV (trochlear), V_1 (ophthalmic), V_2 (maxillary) and VI (abducens), likely exiting through the sphenorbital fissure. This is exhibited by many other placental mammalian orders (e.g., dermopterans, chiropterans, carnivorans; Novacek, 1986, O'Leary et al., 2013). This appears to be the condition for *Tr. hillsii*, *Ti. fodiens, Leptictis* (Novacek, 1986: fig. 30), *E. melanus* (Thewissen and Gingerich, 1989: fig. 7)*, H. lepidus* (Fig. 5G), and possibly *O. tisonensis* (Fig. 5F). The two arctocyonids, *Ad. arenae*, and *Ar. primaevus* (Russell and Sigogneau, 1965), display a different configuration where two separated foramina are present: posterior to the optic canal, the foramen rotundum would have contained V_2 and the sphenorbital fissure would have been for the rest of the nerves and vessels. In *Al. inopinata* (Fig. 5H) and *Ca. coarctatus* (Cameron et al., 2019: fig. 3f), posterior to the optic canal, two separate canals appear to join anteriorly in a common fossa, suggesting an anterior fusion between the foramen rotundum and sphenorbital fissure. We could not identify the condition with certainty for *Ch. baldwini,* and *Pleuraspidotherium*.

Posterior to the sphenorbital fissure, the mandibular nerve (V_3) would have passed through the foramen ovale and is visible in *Tr. hillsii* (Figs. 2D, 3A), *Tr. grangeri* (Figs. 2D, 3C), and *Tr. castoridens* (Figs. 2F, 3E). This would have been the case for all other compared specimens. In lateral view, the exit for V_3 (= foramen ovale) is positioned posteriorly to the cerebrum and not leveled with it in *Trogosus, Ti. fodiens* (Gazin, 1953: fig. 20), *Ar. primaevus* and *Ad. arenae* (Russell and Sigogneau, 1965). In *Al. inopinata*, the exit for V_3 is located on the posterior aspect of the cerebrum (Fig. 5L), while in *O. tisonensis, Ch. baldwini, H. lepidus* (Fig.

5E-G), *Ca. coarctatus* (Cameron et al., 2019: fig. 3f), *Leptictis* (Novacek, 1986: fig. 30), *E. melanus* (Thewissen and Gingerich, 1989: fig. 7), and *Pleuraspidotherium* (Orliac et al., 2012: fig. 4b), it is positioned more anteriorly on the lateral aspect of the cerebrum. The casts for cranial nerves VII (facial) and VIII (vestibulocochlear) could not be reconstructed in any of the *Trogosus* specimens because of lack of preservation.

The cast of the jugular foramen, which would have corresponded to the passageway of the internal jugular vein and cranial nerves IX (glossopharyngeal), X (vagus), and XI (accessory) in life, is visible in all three specimens, *Tr. hillsii* (Figs. 2D, 3B), *Tr. grangeri* (Figs. 2E, 3C), and *Tr. castoridens* (Figs. 2F, 3F). The internal jugular vein cast is positioned anterior to the hypoglossal foramen for cranial nerve XII (hypoglossal). These two features have a similar position in other taxa for which they are both preserved (Fig. 5).

Details of the venous drainage system are visible in all three specimens. In dorsal view, the superior sagittal sulcus that would typically run antero-posteriorly between the cerebral hemispheres cannot be identified in any of the three specimens, *Tr. hillsii* (Fig. 2A), *Tr. grangeri* (Fig. 2B), and *Tr. castoridens* (Fig. 2C). It is also not visible in *Ti. fodiens* but it could be due to the way the endocast was prepared. Compared to other taxa, the superior sagittal sulcus is very subtle in *O. tisonensis* and *Ch. baldwini* (Fig. 5A, B), but this could be due to limited preservation. The other taxa *Al. inopinata*, *H. lepidus* (Fig. 5C, D), *Ar. primaevus, Ad. arenae* (Russell and Sigogneau, 1965), *Leptictis* (Novacek, 1986: fig. 30), and *E. melanus* (Thewissen and Gingerich, 1989: fig. 7) all display a clear superior sagittal sulcus and clear anterior separation between both cerebral hemispheres. The preservation is too limited to make any statement about *Ca. coarctatus* and *Pleuraspidotherium*.

The confluence of sinuses, which would have connected with the superior sagittal and the transverse sinuses, are partially visible in *Tr. hillsii* on the surface of the endocast (Fig. 2A), but not preserved in the two other *Trogosus* specimens. This pattern is typical and present in all fossil taxa preserving this region. The transverse sinus would have abutted the midbrain medially in *H. lepidus* (Fig. 6C)*, Leptictis* (Novacek, 1986: fig. 30), and *E. melanus* (Thewissen and Gingerich, 1989: fig. 7)*,* but the condition in other taxa is not clear because of limited preservation. Laterally, the transverse sinus would have fallen against the lobe of the cerebellum in all taxa. In *Tr. hillsii* (Fig. 2A), it is unclear how much of the transverse sinus would have covered the midbrain because of limited preservation of the area; however, the region where the midbrain lies between the cerebral hemispheres and the cerebellum is relatively long antero-posteriorly.

In the posterior aspect of the endocast, a complex set of large canals surrounds the cerebellum in *Tr. hillsii* (Fig. 4). Some but not all of these canals are also preserved in *Tr. grangeri* (Figs. 2E, 3D) and *Tr. castoridens* (Figs. 2F, 3E-F). Below, we describe what was likely circulating in these canals based on our observations. Comparisons with *Ti. fodiens, O. tisonensis*, and *Ch. baldwini* were not possible because of lack of preservation. Concerning the venous system, the transverse sinus divides into three vessels: the capsuloparietal emissary vein, the sigmoid sinus, and the superior petrosal sinus in eutherians (e.g., Wible, 1984, Novacek, 1986, Muizon et al., 2015). The capsuloparietal emissary vein appears to have connected to the endocranial cavity via the orbitotemporal vein contained into the orbitotemporal canal, visible on the surface of the brain endocast in *Tr. hillsii* (Fig. 4A). This would be similar to the morphology in the pantodont *Al. inopinata* (Muizon et al., 2015: fig. 47), the ‘condylarths’ *H. lepidus, Pleuraspidotherium, Ar. primaevus* (Orliac et al., 2012: fig. 4a, b, e), *Ad. arenae* (Russell and Sigogneau, 1965), and the palaeoryctid *E. melanus* (Wible, 2022: fig. 4). The capsuloparietal

emissary vein would have exited the cranium through the postglenoid foramen as the postglenoid vein in *Tr. hillsii*. This configuration is similar to the condition in *Ca. coarctatus* (Cameron et al., 2019:fig. 3), *Al. inopinata* (Muizon et al., 2015: fig. 47), in the 'condylarths' *H. lepidus, Pleuraspidotherium, Ar. primaevus* (Orliac et al., 2012: fig. 4a, b, e), *Ad. arenae,* the palaeoryctid *E. melanus* (Wible, 2022: fig. 4), and the leptictid *Leptictis* (Novacek, 1986: fig. 28). Part of the capsuloparietal emissary vein cast is preserved in *Tr. grangeri* (Figs. 2E, 3D) and *Tr. castoridens* (Figs. 2F, 3E). The cast for a branch of the capsuloparietal emissary vein, that we interpret as the supraglenoid vein, is also visible and would have exited the cranium through the supraglenoid foramen in *Tr. hillsii* (Fig. 4; see terminology from Cope, 1880). The foramen and the vein cast cannot be identified in the two other *Trogosus* specimens. The cast for the supraglenoid vein is also visible in *Ca. coarctatus* (=sinus drain for the temporomandibular muscles in Cameron et al., 2019:fig. 3) but could not be identified for the remaining of the compared specimens.

Another division of the transverse sinus, the cast of the sigmoid sinus, is visible in *Tr. hillsii* (Fig. 4) and in *Tr. castoridens* (Fig. 3E). The sinus would have run anteroposteriorly on the lateral side of the lateral lobes of the cerebellum and then ventroposteriorly along the cerebellum and would have exited the cranium via the jugular foramen as the internal jugular vein (Wible, 1990). This condition is similar to the pantodont *Al. inopinata* (Muizon et al., 2015: fig. 58), the 'condylarths' *H. lepidus, Pleuraspidotherium, Ar. primaevus* (Orliac et al., 2012: fig. 4a, b, e), *Ad. arenae* (Russell and Sigogneau, 1965), the palaeoryctid *E. melanus* (Wible, 2022: fig. 4), and the leptictid *Leptictis* (Novacek, 1986: fig. 28). The sigmoid sinus would have also connected to the condyloid vein in *Tr. hillsii* (Fig. 4), *Tr. grangeri* (Fig. 2E, 3D), and *Tr. castoridens* (Fig. 2F, 3F). The content of the condyloid canal would have exited through the foramen magnum and would have also been connected to the hypoglossal foramen in all three specimens and in the

compared taxa which preserve this region. The cast for the sigmoid sinus is not preserved in *Tr. grangeri*. There is no evidence of the superior and inferior petrosal sinuses in any of the *Trogosus* specimens.

The cast of the occipital emissary vein can be traced in *Tr. hillsii* (Fig. 4A) and would have exited the endocranial cavity through the mastoid foramen as in the dog (Wible, 2008, Evans and de Lahunta, 2012). This condition would have been similar to *Al. inopinata* for which a mastoid foramen has been identified (Muizon et al., 2015: fig. 53). Finally, the cast of the supraoccipital emissary vein can also be traced in *Tr. hillsii* (Fig. 4A) and would have exited through a foramen that we identify as the supraoccipital foramen. The vein is not preserved in *Tr. grangeri* but may have been present in *Tr. castoridens*; however, it could not be reconstructed with confidence in this specimen. In *Ca. coarctatus*, the vena diploëtica magna, content of the posttemporal canal (= occipital emissary vein in Cameron et al., 2019: fig. 3d) would have exited through the posttemporal foramen, as in *Al. inopinata* (Muizon et al., 2015: fig. 53). There is not evidence of a posttemporal canal in *Trogosus.* In *Leptictis*, the cast of the occipital emissary vein also appears present (mastoid vein in Novacek, 1986) and would have exited posteriorly through the mastoid foramen located in the suture between the supraoccipital, parietal, and petromastoid (Novacek, 1986: fig. 29). The mastoid foramen could not be identified in *E. melanus* (Wible, 2022). The cast of the occipital emissary vein and supraoccipital emissary vein cannot be identified in other compared specimens.

The common carotid artery divides into two branches: the external and internal carotid arteries. The internal carotid artery cast is visible on the surface of the endocast and would have entered the endocranial cavity anterior to the promontorium (Fig. 2D). The stapedial artery, a branch of the internal carotid artery (Fig. 4), would have entered laterally to the promontorium

and given rise to the ramus superior, which is similar to the situation in *E. melanus* (Wible, 2022: fig. 5). There is no evidence of a ramus inferior in *Trogosus*. The ramus superior would have divided into the orbitotemporal artery (=ramus supraorbitalis of Wible, 2022) anteriorly and into a multitude of rami temporales dorsally that can be observed in *Tr. hillsii* (Fig. 4) and in the other specimens of *Trogosus* (Fis. 3D-F). This pattern is similar to that in *E. melanus* (Wible, 2022: figs. 5, 6). The situation is similar in *Al. inopinata* but the cast of the internal carotid artery is not visible on the surface of the brain endocast (Muizon et al., 2015: fig. 57). The majority of the rami temporales would have exited through foramina in the parietal in *Tr. hillsii* and in *E. melanus* (Wible, 2022: fig. 6), while in *Al. inopinata*, they would have exited through the foramina in the squamosal/parietal suture (Muizon et al., 2015: fig: 47). The overall pattern is the same in *Leptictis* (Novacek, 1986: fig. 27), but the rami temporales (sinus canals in Novacek, 1986: fig. 17) would have all exited through the squamosal. Rami temporales are also present in *H. lepidus* but are less numerous.

Relative brain size – Regression lines of the relationship between brain volume and body mass for archaic taxa and crown clades are significantly different (p-value = 0.001; Bertrand et al., 2023, tables S2, S5). The residuals values for *Tr. hillsii* estimated using the Legendre M_1 area (Le) and Damuth M_1 area (DA) equations are slightly below the regression line for the middle Eocene archaic taxa, well below the one for middle Eocene crown clades, and for all taxa (Fig. 7A). The same is true for the residuals generated from the Damuth M_1 length (DL) equation except that it is slightly higher than the regression line for archaic taxa (Fig. 7A). All three residual values for *Tr. hillsii* are close to the early perissodactyl *Hyrachyus modestus* and the mesonychid *Mesonyx obtusidens* (Fig. 7A). In the boxplot of the residuals for the relationship between brain volume and body mass, the three values of *Tr. hillsii* (Le, DA, DL) make this

taxon overlap with *Hyopsodus*, the plesiadapiform *M. annectens,* dinoceratans, and be in the low range of variation for creodonts and carnivoramorphans (Fig. 7B; Bertrand et al., 2023, table S3). Compared to crown clades, the residual value range of *Tr. hillsi* is lower than all middle Eocene crown clades except the primate *Notharctus tenebrosus* with which it overlaps (Fig. 7C; Bertrand et al., 2023, table S3). No groups are significantly different in terms of relative brain size for the middle Eocene crown and archaic groups (Fig. 7C; Bertrand et al., 2023, table S4).

Olfactory bulb size – The olfactory bulb volume percentage for *Tr. hillsii* is 7.3% (Table 2; Bertrand et al., 2023, table S1) and is very close to the perissodactyl *Hyrachuys modestus* (7.9%). Compared to other middle Eocene taxa, *Trogosus* has a higher percentage ratio for the olfactory bulbs compared to all Euarchontoglires (1.0-6.0%), Artiodactyla (4.5-7.0%), the palaeanodont *Metacheiromys marshi* (6.4%), and the dinoceratan *Tetheopsis ingens* (3%). *Trogosus* is on the upper range of variation for Pan-Carnivora (3.8-8.6%). Finally, *Tr. hillsii* has a lower value compared to the 'condylarth' *Hyopsodus* (8.3-8.6%) and the dinoceratan *Uintatherium anceps* (13.7%).

Regression lines of the relationship between olfactory bulb volume and brain volume for archaic taxa and crown clades are significantly different (p-value = 0.003; Bertrand et al., 2023, tables S2, S5). *Trogosus hillsii* is above the regression lines for middle Eocene archaic taxa and all taxa, but below the one for crown clades (Fig. 8A). The residuals from this relationship show that *Tr. hillsii* is very close to the value for the creodont *Cynohaenodon cayluxi* and it overlaps with Carnivoramorpha (Fig. 8B; Bertrand et al., 2023, table S3). Compared to archaic taxa, *Tr. hillsii* has a higher residual value compared to *Microsyops annectens, Sinopa lania*, and *Tetheopsis ingens*, but lower compared to *U. anceps, Hyopsodus, Leptictis*, and *M. marshi* (Fig. 8B). Compared to middle Eocene crown clades, *Tr. hillsii* has a higher value compared to all

taxa except *Hyrachyus modestus* and *Cebochoerus* (Fig. 8C). *Trogosus* has a slightly higher residual value compared to the rodent *Pseudotomus oweni* (Fig. 8C; Bertrand et al., 2023, table S3). Euprimates have significantly lower residuals compared with rodents (p-value = 0.015; Bertrand et al., 2023, table S4) and artiodactyls (p-value = 0.046; Bertrand et al., 2023, table S4).

Regression lines of the relationship between olfactory bulb volume and body mass for archaic taxa and crown clades are not significantly different (p-value = 0.259; Bertrand et al., 2023, tables S2, S5). The residuals values for *Tr. hillsii* estimated using the Legendre M_1 area and Damuth M_1 area equations are slightly above the regression line for archaic taxa and on the line for all taxa (Fig. 8D). The residuals value for *Tr. hillsii* estimated using the Damuth M_1 Length equations is above both archaic and all taxa regression lines. All residuals for *Tr. hillsii* are below the line for crown clades (Fig. 8D; Bertrand et al., 2023, table S3). Compared to archaic groups, the range of *Tr. hillsii* values overlaps with *Hyopsodus*, dinoceratans, creodonts, and the lower range of carnivoramorphans. *Trogosus hillsii* range of values are higher compared to *M. annectens*, but lower than the palaeanodont *M. marshi* (Fig. 8E; Bertrand et al., 2023, table S3). Lastly, compared to crown clades, *Tr. hillsii* overlaps with the lower range of artiodactyls and mid to higher range of rodents. It has a lower value compared to *Hyrachyus modestus*, but higher than euprimates (Fig. 8F; Bertrand et al., 2023, table S3). *Trogosus hillsii* has significantly higher residuals than euprimates (p-value = 0.045; Bertrand et al., 2023, table S4). Euprimates have significantly lower residuals compared to rodents (p-value = 0.027; Bertrand et al., 2023, table S4) and artiodactyls (p-value = 0.045; Bertrand et al., 2023, table S4).

Neocortical size –Trogosus hillsii has a neocortical surface area ratio of 11.46% (Table 2), which is similar to the palaeonodont *M. marshi* (11.47%). *Trogosus hillsii* has a smaller neocortex compared to middle Eocene Euarchontoglires (16.3-43.8%), Pan-Carnivora (16-

25.5%), the perissodactyl *Hyrachyus modestus* (20%), and *Hyopsodus paulus* (13.5%). In terms of the relationship between neocortical surface area and brain surface area, *Tr. hillsii* is below the regression lines for middle Eocene crown clades and archaic taxa (Fig. 9A). *Trogosus hillsii* has a higher residual value compared to the 'condylarth' *Hyopsodus paulus*, the carnivoramorph *Viverravus minutus*, and the palaeanodont *M. marshi*, but lower than the plesiadapiform *M. annectens*, the creodont *S. lania*, other carnivoramorphans, and all crown clades (Fig. 9B, C; Bertrand et al., 2023, table S3). Rodents and euprimates are significantly different in terms of the relative size of the neocortex (p-value = 0.017; Bertrand et al., 2023, table S4).

Endocranial variables and dietary guilds – Herbivorous crown clades have significantly relatively larger brains compared to herbivorous (p-value = 0.003; Bertrand et al., 2023, table S7) and omnivorous-carnivorous archaic groups (p-value = 0.038; Bertrand et al., 2023, table S7). Omnivorous-carnivorous archaic taxa have higher residual average compared to herbivorous archaic groups, but the difference is not significant (p-value = 0.072; Fig. 10A; Bertrand et al., 2023, table S6, S7). Herbivorous crown clades have significantly more expanded neocortices compared to herbivorous archaic groups (p-value = 0.015; Bertrand et al., 2023, table S7) but are in the range of omnivorous-carnivorous archaic groups (p-value = 0.443; Bertrand et al., 2023, table S7). Omnivorous-carnivorous archaic taxa have significantly larger neocortices compared to herbivorous archaic groups (p-value = 0.005; Fig. 10B; Bertrand et al., 2023, table S7). Herbivorous crown clades are in the range of omnivorous-carnivorous archaic groups for the residuals of the olfactory bulb volume against brain volume (p-value = 0.943; Bertrand et al., 2023, table S7). The majority of herbivorous archaic groups overlap with the upper range of herbivore crown clades (p-value = 0.391) and omnivorous-carnivorous archaic groups (p-value = 0.285; Fig. 10C; Bertrand et al., 2023, table S7). When comparing olfactory bulb volume to body

mass, herbivorous crown clades overlap with the upper range of both herbivorous (p-value = 0.528) and omnivorous-carnivorous archaic taxa (p-value = 0.213; Fig. 10D; Bertrand et al., 2023, table S7). The majority of archaic herbivores is in the mid-range of omnivorous-carnivorous archaic groups for the olfactory bulbs against body mass plot (p-value = 0.845; Fig. 10D; Bertrand et al., 2023, table S7). The two extreme datapoints in figure 10C and D are dinoceratans and do not overlap with any other taxa.

Discussion

Endocranial anatomy and phylogenetic relationships

The phylogenetic relationships within Trogosinae remains contentious in part because some taxa are poorly preserved, but also because of a relatively specialized and conserved dentition within the group (e.g., Chow et al., 1996, Miyata, 2007b, Miyata and Deméré, 2016). The monophyly of Trogosinae is not disputed (Rose, 2006), but because of the rarity of well-preserved material, questions remain about the relationships of the seven trogosine species (Miyata and Deméré, 2016). In the most recent phylogenetic analysis, *Tr. hyracoides* and *Tr. castoridens* from Wyoming are sister-taxa, while *Tr. hillsii* and *Tr. grangeri* from Colorado form a clade. However, because both members of each sister-taxon pair co-occur in the same sedimentary basin, some authors have argued that the main morphological difference (i.e., rostrum length) could be attributed to sexual dimorphism (Robinson, 1966). Based on the information obtained from the brain virtual endocasts, we only note one major difference between the species. Gazin (1953) observed only one foramen for both the optic nerve and the content of the sphenorbital fissure in *Tr. grangeri* and *Tr. hillsii*. Miyata and Deméré (2016) noted a similar pattern in *Tr. castoridens*. However, after analyzing the CT data, *Tr. hillsii* appears to

have two distinct foramina (i.e., optic foramen and sphenorbital fissure) as previously observed for *Tillodon fodiens* (Gazin, 1953). Therefore, the fusion of both the sphenorbital fissure and the optic foramen could represent a synapomorphy for *Tr. grangeri* and *Tr. castoridens*. However, it is possible that because of limited preservation of this area, the optic foramen and canal are not preserved in *Tr. grangeri* and *Tr. castoridens*. The condition could not be determined in the CT data of *Tr. hyracoides* because of lack of preservation in this area. *Trogosus grangeri* and *Tr. hillsii* have overall endocranial shapes that are relatively similar but because of the limited preservation of *Tr. castoridens*, we cannot make any firm conclusion about the usefulness of this observation.

Placing Tillodontia on the higher-level family tree of mammals has been challenging, because of a lack of clear synapomorphies uniting the members of this clade with other mammals (Rose, 2006). Tillodonts might have been related to other archaic groups such as Arctocyonidae (Gazin, 1953, Van Valen, 1963, Rose, 1972), but could also potentially be part of Cimolesta (Rose, 2006). However, material of early tillodonts discovered in Asia and their resemblance to Pantodonta led some paleontologists to consider Pantodonta as a more probable sister-clade to Tillodontia (Chow and Wang, 1979, Wang and Jin, 2004). Recently, Muizon et al. (2015) produced a phylogenetic analysis that recovered them as sister-clades. In this analysis, arctocyonids are also relatively closely related to the sister-group of Pantodonta and Tillodontia.

Trogosus displays morphological features that could be interpreted as ancestral for mammals based on what is known of derived conditions present in crown clades. The posterior position of the olfactory bulbs behind the upper molars in *Trogosus*, Taeniodonta, and the 'condylarths' Arctocyonidae and Periptychidae, could represent a plesiomorphic state resulting from the limited development of the brain in these archaic placental mammals. In Eocene crown

clades such as Rodentia and Euprimates (Harrington et al., 2016, Bertrand et al., 2019) the olfactory bulbs are above the tooth row. The circular fissure is also relatively expanded in *Trogosus,* Pantodonta, Taeniodonta, and Arctocyonidae, which could also be considered ancestral. The Eocene crown clades within Euarchontoglires and Artiodactyla have a narrower circular fissure due to the expansion of the frontal lobes of the neocortex onto the circular fissure (Orliac and Gilissen, 2012, Harrington et al., 2016, Bertrand et al., 2019). The absence of sulci on the surface of the neocortex may also represent an ancestral feature related to the limited expansion of the neocortex in *Trogosus* as in *Hyopsodus,* which also displays a lissencephalic brain. Sulci might be present in some archaic taxa (e.g., some plesiadapiforms), but they become more common in crown clades such as Rodentia, Euprimates, and Artiodactyla (Harrington et al., 2016, Bertrand et al., 2019, Orliac et al., 2023). Also related to the development of the neocortex, the more ventral position of the orbitotemporal canal in relation to the rhinal fissure represents an ancestral feature displayed by *Trogosus*, Pantodonta, and Arctocyonidae. The derived condition is present in all crown and archaic Euarchontoglires that preserve both structures and display a complete alignment of the orbitotemporal canal and the rhinal fissure (Silcox et al., 2010, Harrington et al., 2016, Bertrand et al., 2019). The covering of the midbrain has been extensively studied in many mammalian groups (Edinger, 1964). *Trogosus* displays an exposed midbrain, which represents the ancestral condition for mammals. Whether the midbrain is exposed, greatly depends on the development of the neocortex (Dozo et al., 2023), which occurs independently in many different clades (Bertrand et al., 2022).

In terms of possible shared derived endocranial features, *Trogosus, Tillodon*, and arctocyonids share a common position for the exit of V_3, which is located posteriorly to the cerebrum, and in *Alcidedorbignya* it is on the posterior aspect of the cerebrum compared to other

taxa where it is more anteriorly positioned. This feature would not appear to be related to the development of the neocortex. Another characteristic corresponds to the low development of the subarcuate fossa in *Trogosus*, *Alcidedorbignya*, and possibly in the tillodont *Azygonyx* (CT data of UM 68511, see Muizon et al., 2015). *Pantolambda* has identifiable petrosal lobules, but they are smaller than in arctocyonids and taeniodonts (Bertrand et al., 2022). As Muizon et al. (2015) suggested for Pantodonta, relatively reduced subarcuate fossae are probably a derived condition, because they are well developed in Cretaceous taxa such as in early eutherians (i.e., *Kennalestes, Zalambdalestes*; Kielan-Jaworowska, 1984), and in early Laurasiatheria (i.e., *Acmeodon*; Bertrand et al., 2022).

In summary, the endocranial data gathered here show that *Trogosus* displays many ancestral features that are present in other archaic mammals: exposed midbrain, small neocortex, orbitotemporal canal ventral to rhinal fissure, and a broad circular fissure. However, we could identify some potential derived characteristics. Within Trogosinae, we observe variation in the number of foramina and canals for the optic nerve and the content of the sphenorbital fissure. Additionally, the position of the exit of cranial nerve V_3 exit (foramen ovale) and the degree of development of the subarcuate fossa could be characters to add into future phylogenetic analyses aimed at disentangling the intra- and interspecific relationships of Tillodontia.

Endocranial regions and ecological inferences

Trogosus has a very distinctive dentition, including gliriform ever-growing second incisors with restricted enamel similar to rodents (Coombs, 1983). In *Esthonyx*, an early member of the group, the teeth are heavily worn down which would indicate the consumption of abrasive elements such as soil and grit ingested with vegetation pulled out of the ground (Gingerich and Gunnell, 1979). The curved phalanges displayed by tillodonts, including *Trogosus*, are consistent

with digging adaptations (Gazin, 1953, Rose, 1990), suggesting that they might have been using their forelimbs to unearth roots and tubers from underground. *Trogosus* also bears resemblance with clawed herbivores that put more weight on their hind limbs rather than their forelimbs (Coombs, 1983) by having a relatively shorter tibia compared to the femur (Rose, 2006).

Based on the size of the olfactory bulbs and neocortex, *Trogosus* probably relied more on its sense of smell compared to other senses such as vision. Eocene mammals such as early squirrels and euprimates that rely more heavily on vision generally show a posterior expansion of the neocortex (covering of the midbrain) where the occipital cortex is located compared to less derived euarchontoglirans such as plesiadapiforms and ischyromyid rodents (Silcox et al., 2010, Bertrand et al., 2017). The petrosal lobules are also not greatly developed in *Trogosus*, and these structures are known to play a role in maintaining the eye position during movement (Rambold et al., 2002). In contrast, they are greatly expanded in early squirrels, which may have relied on vision while navigating among the complex 3D environment of the trees (Bertrand et al., 2021). A small neocortex has been associated with fossoriality in mammals and more specifically in aplodontiid rodents (Bertrand et al., 2018, 2021) and in the anagalid *An. gobiensis* (López-Torres et al., 2023). In the case of *Trogosus*, because of the lack of data for earlier trogosines, a possible decrease in neocortical surface area related to ecological specialization cannot be tested. Alternatively, as a small neocortex is also the ancestral condition for mammals, the pattern seen in *Trogosus* may simply reflect the ancestral state. Therefore, teasing apart the effect of phylogeny and ecology will require additional data. Nevertheless, endocranial data do not contradict the idea that *Trogosus* was a ground dweller and engaged in digging behavior to unearth roots and tubers. It is challenging to compare the brain of *Trogosus* with modern mammals displaying the same type of feeding behavior, such as Suidae, because they evolved

from early artiodactyls, which had already developed bigger neocortices during the Eocene, probably before any ecological specializations for ground feeding (Orliac and Gilissen, 2012). Overall, this suggests that a complex neocortex was not necessary for the survival of *Trogosus* in its particular ecological niche.

Extinction of Tillodontia and other archaic placental mammals

The extinction of Tillodontia in the Eocene has long been shrouded in mystery. During the Eocene, a time of significant environmental fluctuations, the genus *Esthonyx* shows very limited changes in its lower dental morphology compared to earlier tillodonts, suggesting that this genus and Tillodontia in general may have been more vulnerable to extinction if they were not adapting their dentitions (Luongo et al., 2019). However, this pattern could be interpreted as a morphological specialization which would have potentially be a selective advantage for this genus to allow its survival for more than 7 million years from the late Paleocene to middle Eocene (time range from Lucas and Schoch, 1998). Possible competition for similar resources, both with other archaic placentals and crown species, could have had exacerbated their extinction. The early Eocene taeniodont *Ectoganus copei* appears to have had similar morphological adaptations for digging and hard-object feeding to tillodonts (Coombs, 1983), and the two groups may have overlapped in terms of their ecological niches, putting them in competition for similar resources (Lucas and Schoch, 1998). Tillodontia may also have been in competition with the crown clade Artiodactyla and more specifically with taxa like *Achaenodon*, which displayed similar morphological adaptations (Lucas and Schoch, 1998). This genus was one of the first large artiodactyls that weighted more than 200 kg (Foss, 2001, 2007). No endocranial data have been produced for this taxon but a relatively complete cranium is known (YPM VPPU 010033) and could be CT scanned in the future. Based on published brain virtual

endocasts, the oldest artiodactyl, the early Eocene *Diacodexis* (Orliac and Gilissen, 2012), already had a relatively expanded neocortex that was double the neocortical size of *Trogosus*. Relatively larger brains have been associated with greater behavioral flexibility and may represent a crucial advantage for adapting to new and/or changing environments (Ratcliffe et al., 2006, Sol et al., 2008, 2009, van Woerden et al., 2012). In turn, species with relatively larger brains tend to also have relatively expanded neocortices (Kaas, 2006). Therefore, a bigger neocortex could have provided early artiodactyls with more computational power to access the same resources and adapt more rapidly in response to environmental change.

The extinction of tillodonts may have also been related to predator-prey interaction. Previous studies have hypothesized a possible arms race between mammalian predators and prey in the Paleogene, with an increase in a relative brain size from the Paleocene to the Eocene occurring in parallel in these two guilds (Jerison, 1970, 1973, Bertrand et al., 2022). This hypothesis is supported here by our finding that herbivorous middle Eocene crown clades not only had a relatively larger brain, but also more expanded neocortex compared to herbivorous archaic groups. Furthermore, omnivorous/carnivorous archaic taxa have much larger neocortices compared to herbivorous archaic groups. In light of these findings, it is remarkable that tillodonts retained their relatively small brains and neocortices—inherited from the first placental mammals that radiated after the end-Cretaceous extinction—so deep into the Eocene, when so many other mammals were changing their neurobiology. Therefore, it is possible that tillodonts did not develop the cognitive tools to keep up with the evolution of ever larger-brained and more intelligent predators over evolutionary time, and ever-larger-brained competitor herbivorous species too. Ultimately, the retention of their primitively small brains and neocortices could have

been a factor in the extinction of Tillodontia during the middle Eocene, when competing against artiodactyls for similar resources and avoiding/escaping predators.

Conclusion

The study of the brain endocranial anatomy of *Trogosus* reveals very few anatomical differences among the three species for which we have data. The only potential synapomorphy of a subset of species corresponds to the fusion of both the optic canal and sphenorbital fissure in *Tr. grangeri* and *Tr. castoridens*. Both *Tr. grangeri* and *Tr. hillsii*, which are the best-preserved specimens, are very similar in overall endocranial shape, which reinforces the results from previous work that has struggled to resolve the phylogenetic relationships within *Trogosus* (Chow et al., 1996, Miyata and Deméré, 2016). *Trogosus* displays many ancestral features also present in other archaic taxa: exposed midbrain, small neocortex, orbitotemporal canal ventral to rhinal fissure, and a broad circular fissure. We note two potential characters that might help unite *Trogosus* with Pantodonta and Arctocyonidae: the position of the exit of cranial nerve V_3 exit and the low degree of development of the subarcuate fossa. The relatively large olfactory bulbs and small neocortex of *Trogosus* are consistent with a terrestrial lifestyle and a diet of roots and tubers. The reduced size of the neocortex shows that *Trogosus* did not require an expanded neocortex to survive. However, in addition to dental morphological specializations, a relatively small brain, and particularly neocortex, could have been one of the reasons for the extinction of tillodonts during the middle Eocene. Indeed, competition with contemporary artiodactyls displaying more developed neocortices and increased predation pressure from archaic carnivorans with more developed neocortices could have exacerbated the extinction of tillodonts.

Acknowledgments

This paper began with the Master's thesis of M.J.L. at the University of Edinburgh. We would like to thank K. Miyata and T.A. Deméré for sharing the CT data of *Tr. castoridens* (SDSNH 40829) and M. Hill Chase for assistance in CT scanning the AMNH specimen. This work was supported by Marie Skłodowska-Curie Actions: Individual Fellowship, H2020-MSCA-IF-2018-2020, no. 792611 (O.C.B.); Beatriu de Pinós grant. Expedient number: 2021 BP 00042 (O.C.B). European Research Council (ERC) Starting Grant 756226 under the European Union's Horizon 2020 Research and Innovation Programme (S.L.B.); Philip Leverhulme Prize (S.L.B.); NSF DEB 1654952 (T.E.W. and S.L.B.); NSF DEB 1654949 (J.R.W.). There is no conflict of interest. We would like to thank two anonymous reviewers and Philip Cox for their helpful suggestions and comments.

Author contributions

O.C.B., M.J.L., and S.L.B. conceived and designed the study. O.C.B., and M.J. (AMNH specimen), and J.R.W (USNM specimen) acquired the CT data. O.C.B. and M.J.L. did all segmentations and drafted the manuscript, tables, and figures. Analyses and interpretations were performed by O.C.B., and M.J.L. and critically reviewed by S.L.B., S.L.S., J.R.W., T.E.W., and M.J.L. All authors revised the manuscript and provided final approval before submission.

Data Availability Statement

The code to reproduce the analyses is on the Github Repository: https://github.com/Bertrand-Ornella/Trogosus-Brain-evolution-Archaic-Mammals, and the brain virtual endocasts for the different specimens of *Trogosus* are accessible in MorphoSource: https://www.morphosource.org/projects/000519068?locale=en.

References

Benoit J, Crumpton N, Mérigeaud S, Tabuce R (2013) A memory already like an elephant's? The advanced brain morphology of the last common ancestor of Afrotheria (Mammalia). *Brain Behav. Evol.,* **81,** 154-169.

Bertrand OC, Amador-Mughal F, Lang MM, Silcox MT (2018) Virtual endocasts of fossil Sciuroidea: brain size reduction in the evolution of fossoriality. *Palaeontology,* **61,** 919-948.

Bertrand OC, Amador-Mughal F, Lang MM, Silcox MT (2019) New virtual endocasts of Eocene Ischyromyidae and their relevance in evaluating neurological changes occurring through time in Rodentia. *J. Mamm. Evol.,* **26,** 345-371.

Bertrand OC, Amador-Mughal F, Silcox MT (2016) Virtual endocasts of Eocene *Paramys* (Paramyinae): oldest endocranial record for Rodentia and early brain evolution in Euarchontoglires. *Proc. R. Soc. B,* **283**.

Bertrand OC, Amador-Mughal F, Silcox MT (2017) Virtual endocast of the early Oligocene *Cedromus wilsoni* (Cedromurinae) and brain evolution in squirrels. *J. Anat.,* **230,** 128-151.

Bertrand OC, Jimenez Lao M, Shelley SL, et al. (2023) Data from: The virtual brain endocast of *Trogosus* (Tillodontia) and its relevance in understanding the extinction of archaic placental mammals. *Dryad Digital Repository*.

Bertrand OC, Püschel HP, Schwab JA, Silcox MT, Brusatte SL (2021) The impact of locomotion on the brain evolution of squirrels and close relatives. *Commun. Biol,* **4,** 1-15.

Bertrand OC, Shelley SL, Wible JR, et al. (2020) Virtual endocranial and inner ear endocasts of the Paleocene 'condylarth' *Chriacus*: new insight into the neurosensory system and evolution of early placental mammals. *J. Anat.,* **236,** 21-49.

Bertrand OC, Shelley SL, Williamson TE, et al. (2022) Brawn before brains in placental mammals after the end-Cretaceous extinction. *Science,* **376,** 80-85.

Bertrand OC, Silcox MT (2016) First virtual endocasts of a fossil rodent: *Ischyromys typus* (Ischyromyidae, Oligocene) and brain evolution in rodents. *J. Vertebr. Paleontol,* **36**.

Cameron J, Shelley SL, Williamson TE, Brusatte SL (2019) The brain and inner ear of the early Paleocene “condylarth” *Carsioptychus coarctatus*: implications for early placental mammal neurosensory biology and behavior. *Anat. Rec.,* **302,** 306-324.

Chambers JM, Hastie TJ (1992) *Statistical Models in S*, London: Chapman & Hall.

Chow M-C, Wang JP, Meng JP (1996) A new species of *Chungchienia* (Tillodontia, Mammalia) from the Eocene of Lushi, China. *Am. Mus. Novit.,* **3171,** 1-10.

Chow M, Wang B (1979) Relationship between the pantodonts and tillodonts and classification of the order Pantodonta. *Vertebr. Palasiat.,* **17,** 37-48.

Coombs MC (1983) Large mammalian clawed herbivores: a comparative study. *Trans. Am. Philos. Soc.,* **73,** 1-96.

Cope ED (1877) On the brain of *Coryphodon*. *Proc. Am. Philos. Soc.,* **16,** 616-620.

Cope ED (1880) On the foramina perforating the posterior part of the squamosal bone of the Mammalia. *Proc. Am. Philos. Soc.,* **18,** 452-461.

Dag O, Dolgun A, Konar NM (2018) Onewaytests: an R Package for one-way tests in independent groups designs. *R Journal,* **10,** 175-199.

Damuth J (1990) Problems in estimating body masses of archaic ungulates using dental measurements. In *Body Size in Mammalian Paleobiology: Estimation and Biological*

Implications (eds Damuth J, MacFadden BJ), pp. 229–253. Cambridge: Cambridge University Press.
Dozo MT, Paulina-Carabajal A, Macrini TE, Walsh S (2023) *Paleoneurology of Amniotes: New Directions in the Study of Fossil Endocasts*, Cham: Springer International Publishing.
Edinger T (1929) *Die fossilen Gehirne. ErgebAnatB. Entwicklungsgesch 28*, Berlin: Julius Springer Verlag.
Edinger T (1964) Midbrain exposure and overlap in mammals. *Am. Zool.,* **4,** 5-19.
Eisenberg JF (1981) *The Mammalian Radiations: an Analysis of Trends in Evolution, Adaptation, and Behavior*, Chicago: University of Chicago Press.
Evans HE, de Lahunta A (2012) *Miller's Anatomy of the Dog*, St. Louis, USA: Elsevier Saunders.
Foss SE (2001) Systematics and paleobiology of the Entelodontidae (Mammalia, Artiodactyla). Ph.D. Thesis, DeKalb: Northern Illinois University.
Foss SE (2007) Family Helohyidae. In *The evolution of artiodactyls* (eds Prothero DR, Foss SE), pp. 85-88. Baltimore: John Hopkins University Press.
Gazin CL (1953) The Tillodontia, an early Tertiary order of mammals. *Smithson. Misc. Collect.,* **121,** 1-134.
Gingerich PD, Gunnell GF (1979) Systematics and evolution of the genus *Esthonyx* (Mammalia, Tillodontia) in the early Eocene of North America. *Contrib. Mus. Paleontol. Univ. Mich.,* **25,** 125–153.
Group VS (1995-2019) Avizo Lite 2019.4, Berlin (ZIB), Germany: Konrad-Zuse-Zentrum für Informationstechnik.
Harrington AR, Silcox MT, Yapuncich GS, Boyer DM, Bloch JI (2016) First virtual endocasts of adapiform primates. *J. Hum. Evol.,* **99,** 52-78.
Harrington AR, Yapuncich G, Boyer D (2020) The digital endocast of *Necrolemur antiquus*. *Palaeovertebrata,* **43,** 1-10.
Hothorn T, Hornik K, van de Wiel M, Zeileis A (2006) A Lego system for conditional inference. *The American Statistician,* **60,** 257–263.
Jerison HJ (1961) Quantitative analysis of evolution of the brain in mammals. *Science,* **133,** 1012-1014.
Jerison HJ (1970) Brain evolution: new light on old principles. *Science,* **170,** 1224-1225.
Jerison HJ (1973) *Evolution of the Brain and Intelligence*, New York: Academic Press.
Jerison HJ (2012) Digitized fossil brains: neocorticalization. *Biolinguistics,* **6,** 383-392.
Kaas JH (2006) Evolution of the neocortex. *Current Biology,* **16,** R910-R914.
Kielan-Jaworowska Z (1984) Evolution of the therian mammals in the Late Cretaceous of Asia. Part VI. Endocranial casts of eutherian mammals. *Acta Palaeontol. Pol.,* **46,** 157-171.
Kirk EC, Daghighi P, Macrini TE, Bhullar BS, Rowe TB (2014) Cranial anatomy of the Duchesnean primate *Rooneyia viejaensis*: new insights from high resolution computed tomography. *J. Hum. Evol.,* **74,** 82-95.
Lang MM, Bertrand OC, San Martin-Flores G, et al. (2022) Scaling patterns of cerebellar petrosal lobules in Euarchontoglires: impacts of ecology and phylogeny. *Anat. Rec.,* **305,** 3472-3503.
Legendre S (1989) Les communautés de mammifères du Paléogène (Eocène supérieur et Oligocène) d'Europe occidentale: structures, milieux et évolution. *Münch. Geowiss. Abh. (A),* **16,** 1-110.
Leidy J (1871) Remains of extinct mammals from Wyoming. *Proc. Acad. Nat. Sci. Phila.,* **23,** 113-116.

Long A, Bloch JI, Silcox MT (2015) Quantification of neocortical ratios in stem primates. *Am. J. Phys. Anthropol.,* **157,** 363-73.
López-Torres S, Bertrand OC, Lang MM, Silcox MT, Fostowicz-Frelik Ł, Meng J (2023) Cranial endocast of *Anagale gobiensis* (Anagalidae) and its implications for early brain evolution in Euarchontoglires. *Palaeontology,* **66,** e12650.
Lucas S, Schoch R (1998) Tillodontia. In *Evolution of Tertiary Mammals of North America: Volume 1, Terrestrial Carnivores, Ungulates, and Ungulate Like Mammals* (eds Janis CM, Scott KM, Jacobs LL, Gunnell GF, Uhen MD), pp. 268-273. Cambridge: Cambridge University Press.
Lucas SG (1993) Pantodonts, tillodonts, uintatheres, and pyrotheres are not ungulates. In *Mammal phylogeny* (eds Szalay FS, Novacek MJ, McKenna MC), pp. 182-194. New York: Springer-Verlag.
Luongo RA, Cozart HK, Ahrens HE (2019) Patterns of dental morphology and disparity in the Eocene herbivore lineage *Esthonyx* (Mammalia, Tillodontia). *The FASEB Journal,* **33,** 614.3-614.3.
Mangiafico S (2017) rcompanion: functions to support extension education program evaluation, New Brunswick, New Jersey: Rutgers Cooperative Extension. https://CRAN.R-project.org/package=rcompanion/.
Marsh OC (1876) Principal characters of the Tillodontia. *Am. J. Sci. Arts.,* **11,** 249-251.
Martin RD (1990) Evolution of the primate central nervous system. In *Primate Origins and Evolution. A Phylogenetic Reconstruction*), pp. 357-426. Princeton: Princeton University Press.
Maugoust J, Orliac MJ (2021) Endocranial cast anatomy of the extinct hipposiderid bats *Palaeophyllophora* and *Hipposideros* (*Pseudorhinolophus*) (Mammalia: Chiroptera). *J. Mamm. Evol.,* **28,** 679-706.
McKenna MC, Bell SK (1997) *Classification of Mammals: Above the Species Level*, New York: Columbia University Press.
Meng J, Hu Y, Li C (2003) The osteology of *Rhombomylus* (Mammalia, Glires): implications for phylogeny and evolution of Glires. *Bull. Am. Mus. Nat. Hist.,* **2003,** 1-247.
Miyata K (2007a) New material of Asian *Trogosus* (Tillodontia, Mammalia) from the Akasaki Formation, Kumamoto Prefecture, Japan. *J. Vertebr. Paleontol,* **27,** 176-188.
Miyata K (2007b) New species of *Trogosus* (Tillodontia, Mammalia) from the Green River Basin, Wyoming, U.S.A. *J. Vertebr. Paleontol,* **27,** 661-675.
Miyata K, Deméré TA (2016) New material of a 'short-faced' *Trogosus* (Mammalia, Tillodontia) from the Delmar Formation (Bridgerian), San Diego County, California, U.S.A. *J. Vertebr. Paleontol,* **36,** e1089878.
Muizon C, Billet G, Argot C, Ladevèze S, Goussard F (2015) *Alcidedorbignya inopinata*, a basal pantodont (Placentalia, Mammalia) from the early Palaeocene of Bolivia: anatomy, phylogeny and palaeobiology. *Geodiversitas,* **37,** 397-634.
Napoli JG, Williamson TE, Shelley SL, Brusatte SL (2018) A digital endocranial cast of the early Paleocene (Puercan) 'archaic'mammal *Onychodectes tisonensis* (Eutheria: Taeniodonta). *J. Mamm. Evol.,* **25,** 179-195.
Novacek MJ (1982) The brain of *Leptictis dakotensis*, an Oligocene leptictid (Eutheria: Mammalia) from North America. *J. Paleontol.,* **56,** 1177-1186.
Novacek MJ (1986) The skull of leptictid insectivorans and the higher-level classification of eutherian mammals. *Bull. Am. Mus. Nat. Hist.,* **183,** 1-112.

O'Leary MA, Bloch JI, Flynn JJ, et al. (2013) The placental mammal ancestor and the post-K-Pg radiation of placentals. *Science,* **339,** 662-7.
Orliac MJ, Argot C, Gilissen E (2012) Digital cranial endocast of *Hyopsodus* (Mammalia, "Condylarthra"): a case of paleogene terrestrial echolocation? *PloS one,* **7,** e30000-e30000.
Orliac MJ, Gilissen E (2012) Virtual endocranial cast of earliest Eocene *Diacodexis* (Artiodactyla, Mammalia) and morphological diversity of early artiodactyl brains. *Proc. R. Soc. B,* **279,** 3670-3677.
Orliac MJ, Ladevèze S, Gingerich PD, Lebrun R, Smith T (2014) Endocranial morphology of Palaeocene *Plesiadapis tricuspidens* and evolution of the early primate brain. *Proc. R. Soc. B,* **281,** 20132792.
Orliac MJ, Maugoust J, Balcarcel A, Gilissen E (2023) Paleoneurology of Artiodactyla, an overview of the evolution of the artiodactyl brain. In *Paleoneurology of Amniotes : New Directions in the Study of Fossil Endocasts* (eds Dozo MT, Paulina-Carabajal A, Macrini TE, Walsh S), pp. 507-555. Cham: Springer International Publishing.
Perini FA, Macrini TE, Flynn JJ, et al. (2022) Comparative endocranial anatomy, encephalization, and phylogeny of Notoungulata (Placentalia, Mammalia). *J. Mamm. Evol.,* **29,** 369-394.
Pinheiro J, Bates D, DebRoy S, Sarkar D (2018) nlme: linear and nonlinear mixed effects models: R package version 3.1-131.1. https://CRAN.R-project.org/package=nlme.
Rambold H, Churchland A, Selig Y, Jasmin L, Lisberger SG (2002) Partial ablations of the flocculus and ventral paraflocculus in monkeys cause linked deficits in smooth pursuit eye movements and adaptive modification of the VOR. *J. Neurophysiol.,* **87,** 912-924.
Ramdarshan A, Orliac MJ (2016) Endocranial morphology of *Microchoerus erinaceus* (Euprimates, Tarsiiformes) and early evolution of the Euprimates brain. *Am. J. Phys. Anthropol.,* **159,** 5-16.
Ratcliffe JM, Fenton MB, Shettleworth SJ (2006) Behavioral flexibility positively correlated with relative brain volume in predatory bats. *Brain Behav. Evol.,* **67,** 165-176.
RCoreTeam (2019) R: A language and environment for statistical computing., Vienna, Austria: R Foundation for Statistical Computing. https://www.R-project.org/.
Robinson P (1966) Fossil Mammalia of the Huerfano Formation, Eocene, of Colorado. *Bull. Yale Peabody Mus.,* **21**.
Rose K (2001) Compendium of Wasatchian mammal postcrania from the Willwood Formation. In *Paleocene-Eocene Stratigraphy and Biotic Change in the Bighorn and Clarks Fork Basins of Northwestern Wyoming* (ed Gingerich PD), pp. 157–183. Ann Arbor: University of Michigan Papers on Paleontology.
Rose KD (1972) A new tillodont from the Eocene upper Willwood Formation of Wyoming. *Postilla,* **155,** 1-13.
Rose KD (1990) Postcranial skeletal remains and adaptations in early Eocene mammals from the Willwood Formation, Bighorn Basin, Wyoming. *Geol. Soc. Am. Spec. Pap.,* **243,** 107-133.
Rose KD (2006) *The Beginning of the Age of Mammals*, Baltimore: Johns Hopkins University Press.
Rose KD, Kumar K, Rana RS, Sahni A, Smith T (2013) New hypsodont tillodont (Mammalia, Tillodontia) from the early Eocene of India. *J. Paleontol.,* **87,** 842-853.

Rose KD, Rana RS, Sahni A, Kumar K, Singh L, Smith T (2009) First tillodont from India: additional evidence for an early Eocene faunal connection between Europe and India? *Acta Palaeontol. Pol.,* **54,** 351-355, 5.
RStudioTeam (2022) RStudio: Integrated Development Environment for R, Boston: Rstudio, PBC. http://www.rstudio.com.
Russell DE, Sigogneau D (1965) Étude de moulages endocrâniens de mammifères paléocènes. *Mém. Mus. natl. hist. nat., Sér. C Géol.,* **16**.
Schoch RM (1983) An endocranial cast of *Ectoganus*, an early Tertiary taeniodont. *J. Mammal.,* **64,** 180-183.
Silcox MT, Benham AE, Bloch JI (2010) Endocasts of *Microsyops* (Microsyopidae, Primates) and the evolution of the brain in primitive primates. *J. Hum. Evol.,* **58,** 505-21.
Silcox MT, Dalmyn CK, Bloch JI (2009) Virtual endocast of *Ignacius graybullianus* (Paromomyidae, Primates) and brain evolution in early primates. *Proc. Natl. Acad. Sci. USA,* **106,** 10987-10992.
Silcox MT, Dalmyn CK, Hrenchuk A, Bloch JI, Boyer DM, Houde P (2011) Endocranial morphology of *Labidolemur kayi* (Apatemyidae, Apatotheria) and its relevance to the study of brain evolution in Euarchontoglires. *J. Vertebr. Paleontol,* **31,** 1314-1325.
Sol D (2009) Revisiting the cognitive buffer hypothesis for the evolution of large brains. *Biol. Lett.,* **5,** 130-133.
Sol D, Bacher S, Reader Simon M, Lefebvre L (2008) Brain size predicts the success of mammal species introduced into novel environments. *The American Naturalist,* **172,** S63-S71.
Szalay FS (1977) Phylogenetic relationships and a classification of the eutherian Mammalia. In *Major Patterns in Vertebrate Evolution* (eds Hecht MK, Goody PC, Hecht BM), pp. 315-374. Boston: Springer.
Thewissen JGM, Gingerich PD (1989) Skull and endocranial cast of *Eoryctes melanus*, a new palaeoryctid (Mammalia: Insectivora) from the early Eocene of western North America. *J. Vertebr. Paleontol,* **9,** 459-470.
Van Valen L (1963) The origin and status of the mammalian order Tillodontia. *J. Mammal.,* **44,** 364-373.
van Woerden JT, Willems EP, van Schaik CP, Isler K (2012) Large brains buffer energetic effects of seasonal habitats in catarrhine primates. *Evolution,* **66,** 191-199.
Wang Y, Jin X (2004) A new Paleocene tillodont (Tillodontia, Mammalia) from Qianshan, Anhui, with a review of Paleocene tillodonts from China. *Vertebr. Palasiat.,* **42,** 14-26.
Welch BL (1951) On the comparison of several mean values: an alternative approach. *Biometrika,* **38,** 330-336.
White CL, Bloch JI, Morse PE, Silcox MT (2023) Virtual endocast of late Paleocene *Niptomomys* (Microsyopidae, Euarchonta) and early primate brain evolution. *J. Hum. Evol.,* **175,** 103303.
Wible JR (1984) The ontogeny and phylogeny of the mammalian cranial arterial pattern. Ph.D. Thesis, Durham: Duke University.
Wible JR (1987) The eutherian stapedial artery: character analysis and implications for superordinal relationships. *Zool. J. Linnean Soc.,* **91,** 107-135.
Wible JR (1990) Petrosals of Late Cretaceous marsupials from North America, and a cladistic analysis of the petrosal in therian mammals. *J. Vertebr. Paleontol,* **10,** 183-205.

Wible JR (2008) On the cranial osteology of the Hispaniolan solenodon, *Solenodon paradoxus* Brandt, 1833 (Mammalia, Lipotyphla, Solenodontidae). *Ann. Carnegie Mus.,* **77,** 321-402.
Wible JR (2022) Petrosal and cranial vascular system of the early Eocene palaeoryctid *Eoryctes melanus* from northwestern Wyoming, USA. *Acta Palaeontol. Pol.,* **67,** 203-220.
Wickham H (2016) *ggplot2: Elegant Graphics for Data Analysis*, New York: Springer-Verlag.

Tables

Table 1. Equations used to calculate the body masses of *Trogosus hillsii* (USNM 17157). Abbreviations: BM, body mass; CL, cranial length; EXP, exponential; LN, natural logarithm; LOG10, logarithm with base 10; m1, lower molar 1. Specimen used for estimating body mass: USNM 17157 (Miyata, 2007a).

Formula	r2	References	Body mass (kg)
10^(3.17 x (LOG10(m1 length)) + 1.04)	0.98	Damuth (1990) - Non selenodont taxa	66.41
10^(1.51 x (LOG10(m1 area))+1.44)	0.97	Damuth (1990) - Non selenodont taxa	97.38
EXP(1.7054 x (LN(m1 area)) + 2.247)	0.97	Legendre (1989) - Mammals	96.27

Table 2. Linear measurements, volumes and surface areas for the different endocasts of *Trogosus* described in this study. Values with the asterisk * are estimations.

	Trogosus hillsii USNM 17157	*Trogosus grangeri* AMNH FM 17008	*Trogosus castoridensis* SDSNH 40819
Measurements (mm)			
Total endocast length (TL)	82.78	-	-
Olfactory bulbs length (OL)	18.44	-	-
Olfactory bulbs width (OW)	32.17	-	-
Olfactory bulbs height (OH)	20.01	-	-
Cerebrum maximal length (CRML)	34.52*	38.1*	26.84*
Cerebrum maximal width (CRMW)	49.24	48.28	25.6*
Cerebrum maximal height (CRMH)	32.76	34.43	-
Cerebellum width (CLW)	47.67	43.60	25.47*
Cerebellum maximal length (CLML)	17.85*	17.11*	9.2*
Ratios linear measurements (%)			
OL/TL	22.28	-	-
CRML/TL	41.70	41.65	-
CLML/TL	21.56	18.71	-
CLW/CRMW	96.81	90.31	99.49
OW/CRMW	65.33	-	-
OW/CLW	67.48	-	-
Surface areas (mm^2) and volumes (mm^3)			
Total endocast surface area	12676.30	18170.63*	-
Neocortical surface area	1313.58	-	-
Total endocast volume	61021.20	-	-
Olfactory bulbs volume	4428.85	-	-
Ratios surface areas and volumes (%)			
NS/TS	10.36	-	-
OV/TV	7.26	-	-

Figure captions

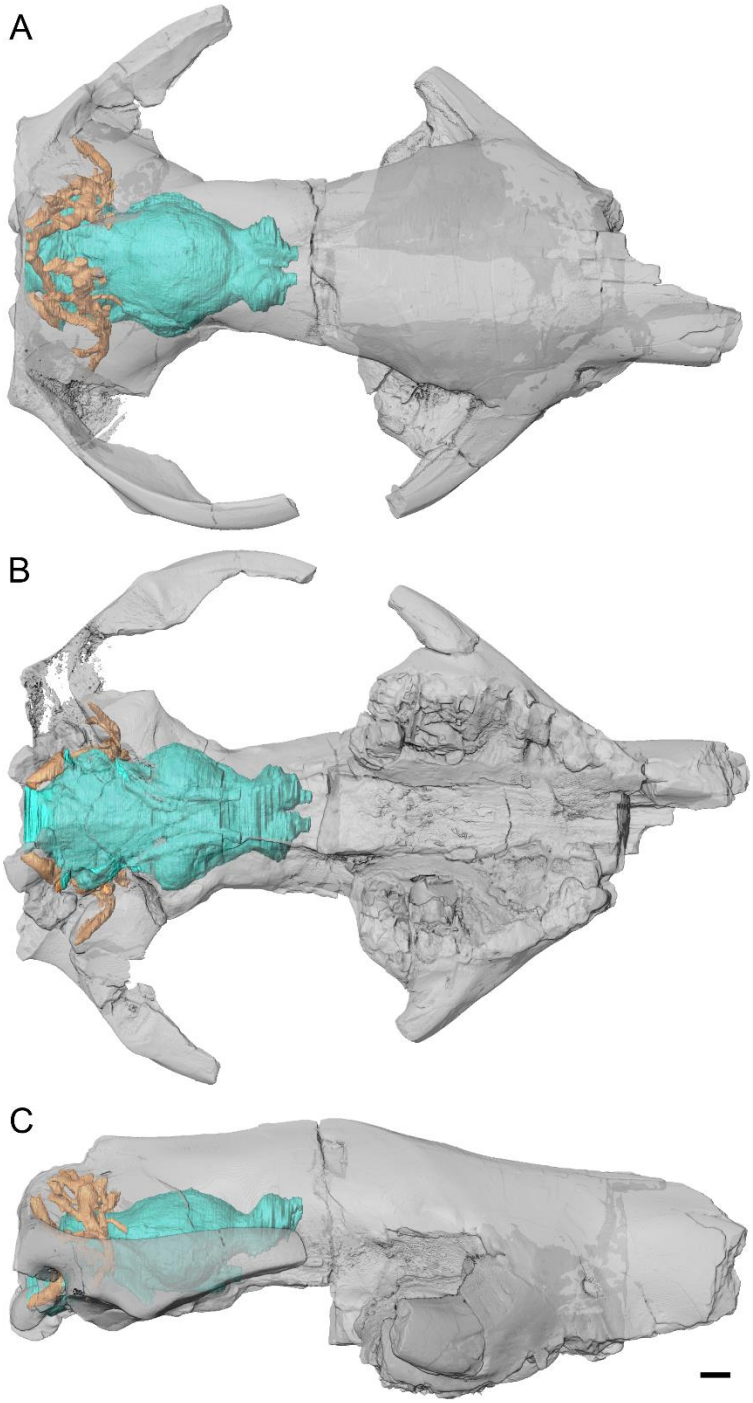

Figure 1. Virtual endocasts inside the cranium of *Trogosus hillsii* (USNM 17157). A. Dorsal, B. ventral and C. lateral views. Scale = 10 mm.

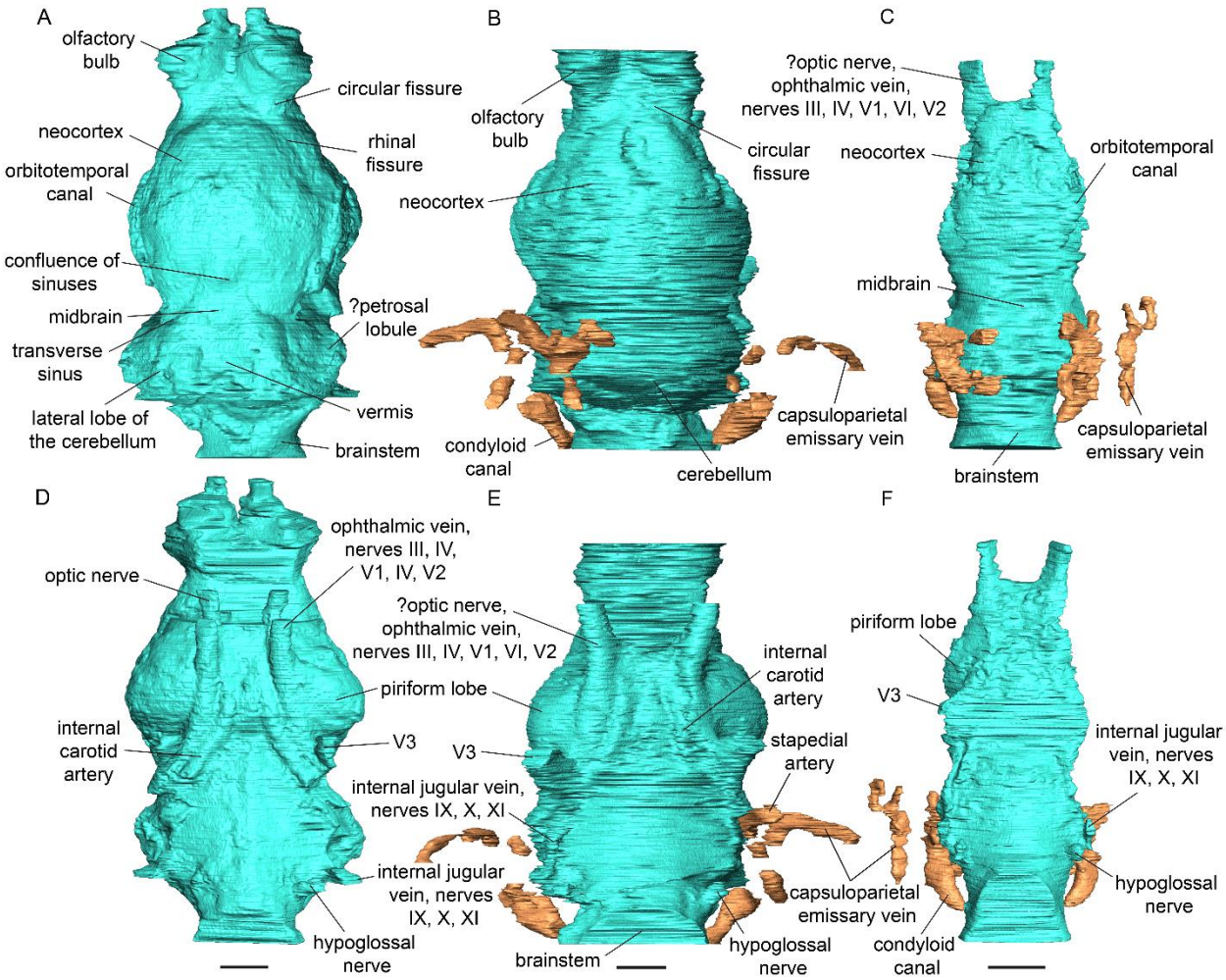

Figure 2. Virtual reconstructions in dorsal and ventral views of the brain endocast of A., D. *Trogosus hillsii* (USNM 17157), B., E. *Trogosus grangeri* (AMNH FM 17008), and C., F. *Trogosus castoridens* (SDSNH 40819). Scale = 10 mm.

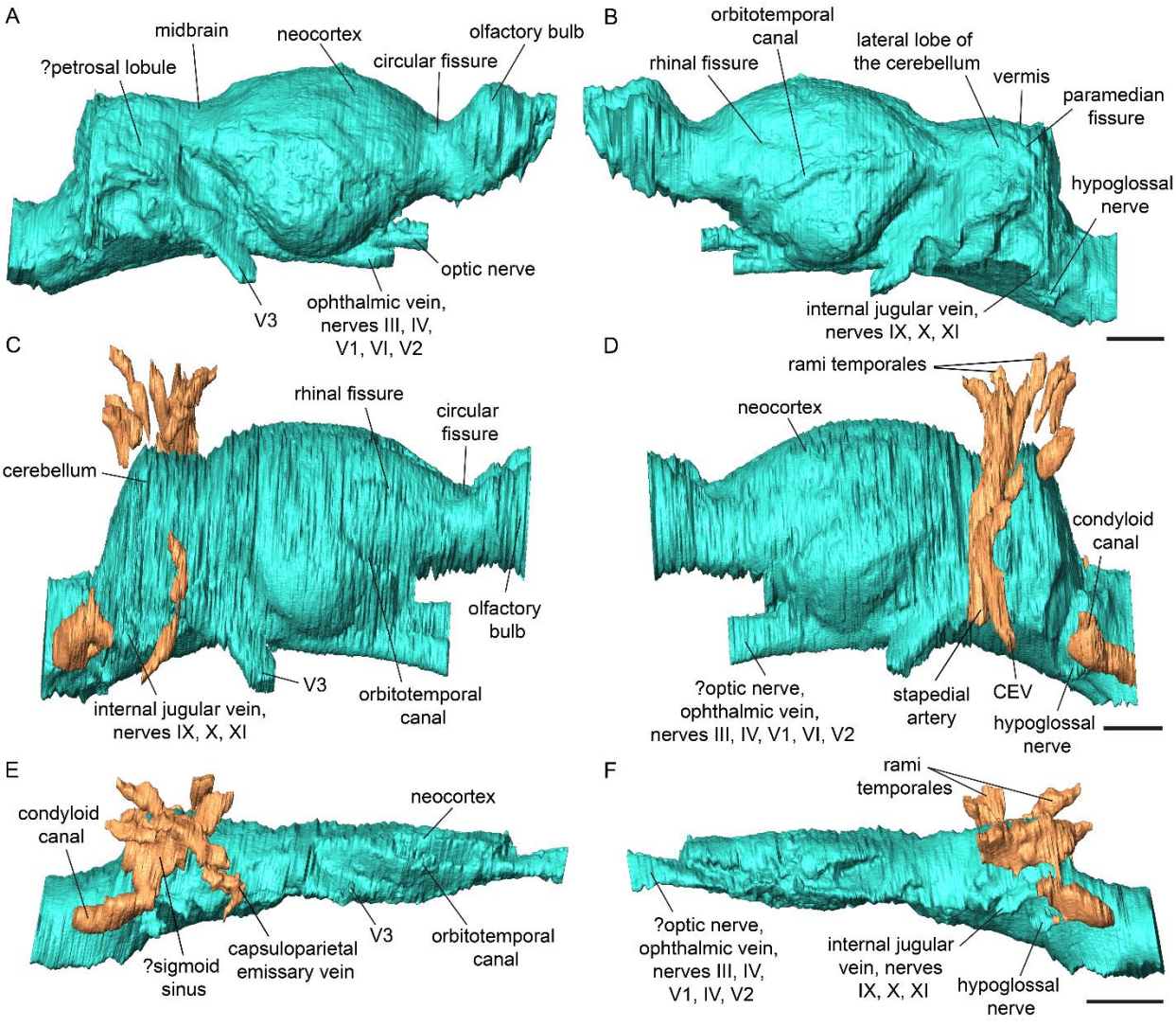

Figure 3. Virtual reconstructions in lateral views of the brain endocast of A., B. *Trogosus hillsii* (USNM 17157), C., D. *Trogosus grangeri* (AMNH FM 17008), and E., F. *Trogosus castoridens* (SDSNH 40819). Scale = 10 mm.

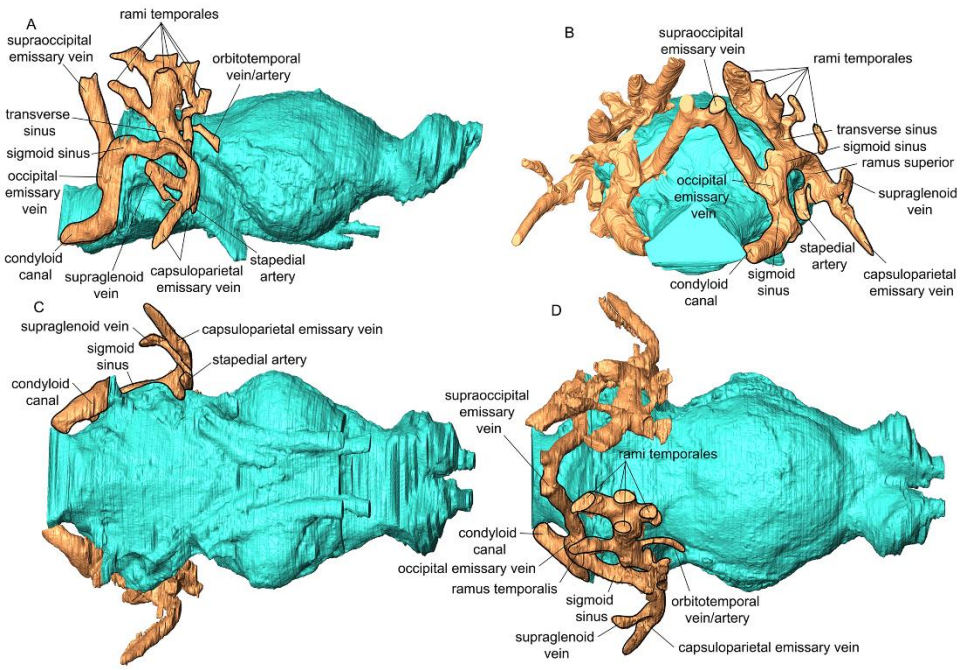

Figure 4. Virtual reconstruction of the brain endocast and canals for blood vessels in *Trogosus hillsii* (USNM 17157). A. lateral, B. posterior, C. ventral, and D. dorsal views. Scale = 10 mm.

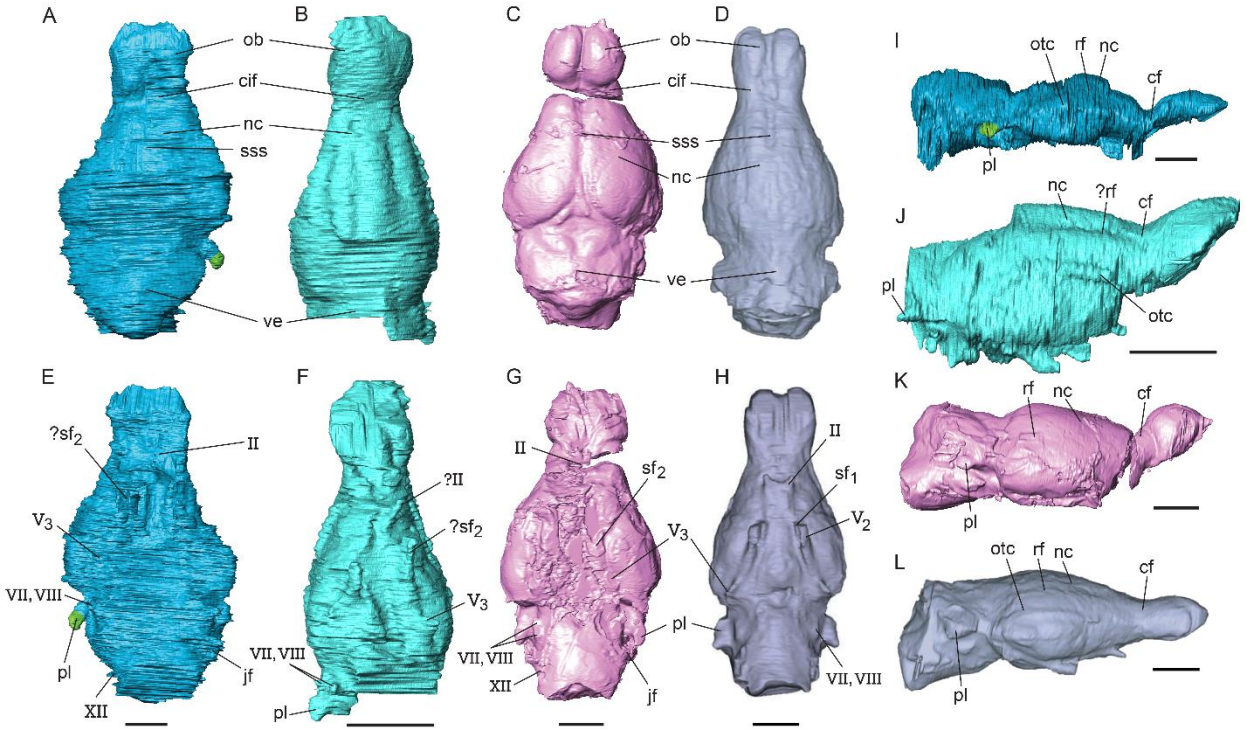

Figure 5. Virtual endocasts of compared archaic mammals. *Chriacus baldwini* (MCZ 20676; Bertrand et al., 2020) in A. dorsal, E. ventral, and I. lateral views. *Onychodectes tisonensis* (AMNH 785; Napoli et al., 2017) in B. dorsal, F. ventral, and J. lateral views. *Hyopsodus lepidus* (AMNH FM 143783) in C. dorsal, G. ventral, and K. lateral views. *Alcidedorbignya inopinata* (MHNC 8372; Muizon et al., 2015) in D. dorsal, H. lateral, and L. ventral views. **Abbreviations:** cif, circular fissure; jf, internal jugular vein and cranial nerves IX, X, XI; nc, neocortex; ob, olfactory bulb; otc, orbitotemporal canal; II, optic nerve; pl, petrosal lobule; rf, rhinal fissure; sf_1, ophthalmic veins and cranial nerves III, IV, V_1, and VI; sf_2, ophthalmic veins and cranial nerves III, IV, V_1, V_2 and VI; sss, superior sagittal sulcus; ve, vermis; V_2, maxillary nerve; V_3, mandibular nerve; VII, facial nerve; VIII, vestibulocochlear nerve; XII, hypoglossal nerve. Scale = 10 mm.

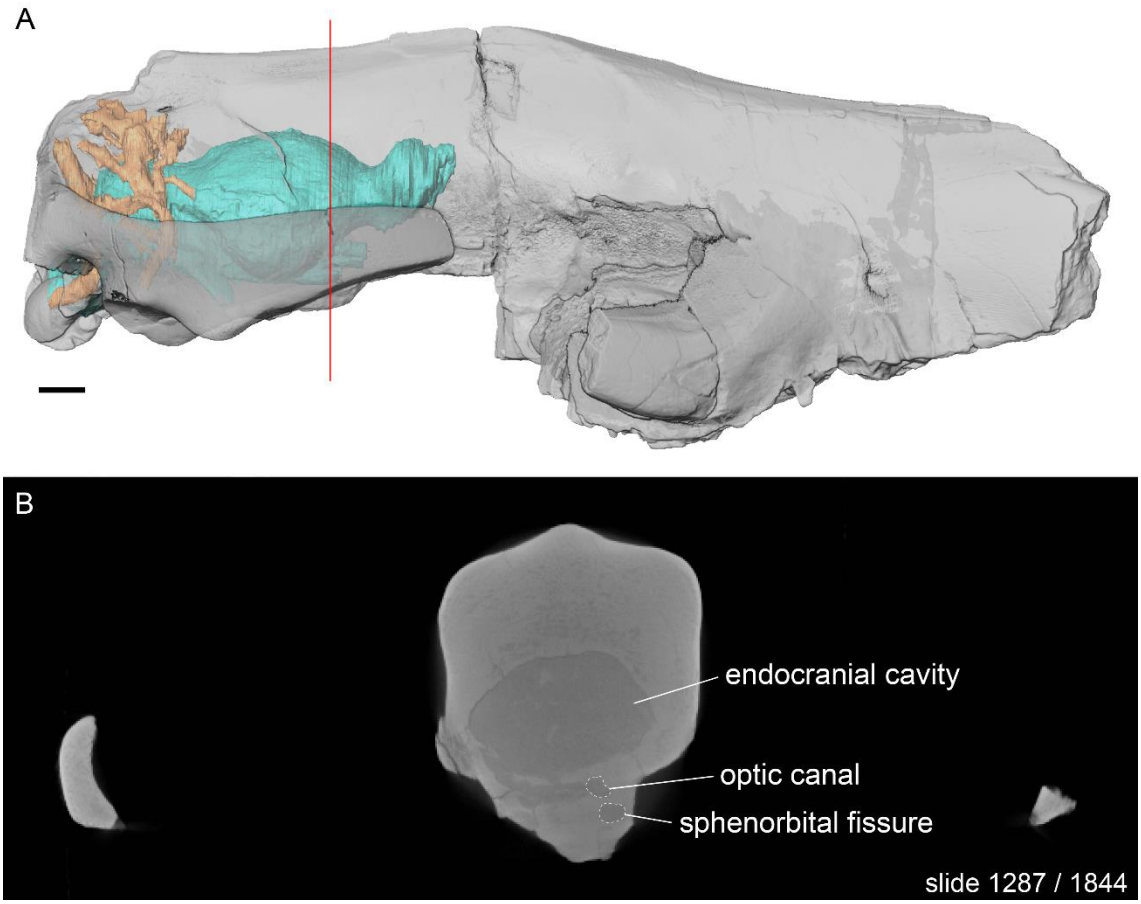

Figure 6. Cranium of *Trogosus hillsii* (USNM 17157). A. lateral view of the cranium. B. CT cross-sectional view of the braincase. The line in A denotes the plane of the cross-sectional view (Slice 1287).

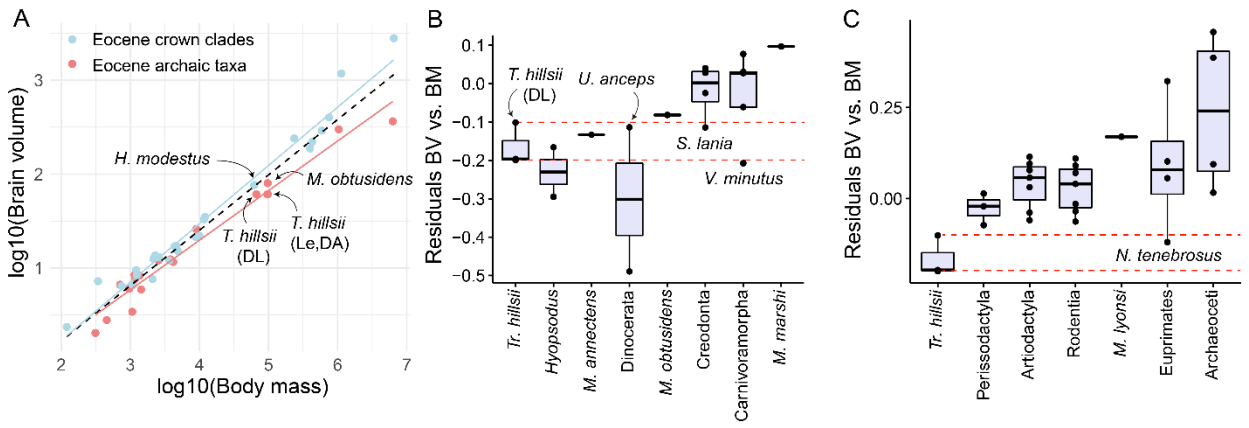

Figure 7. Relative size of the brain of middle Eocene mammals. A. Linear regression of log10 (Endocranial volume area vs. Body mass) for archaic groups and crown clades, B. Boxplot of the residuals from the equation in A. for *Trogosus* and other archaic groups, C. Boxplot of the residuals from the equation in A. for *Trogosus* and crown clades. See table S2 for residual values. Volumetric measurements are in cubic centimeters and body mass was measured in grams. **Abbreviations:** BM, body mass; BV, brain volume.

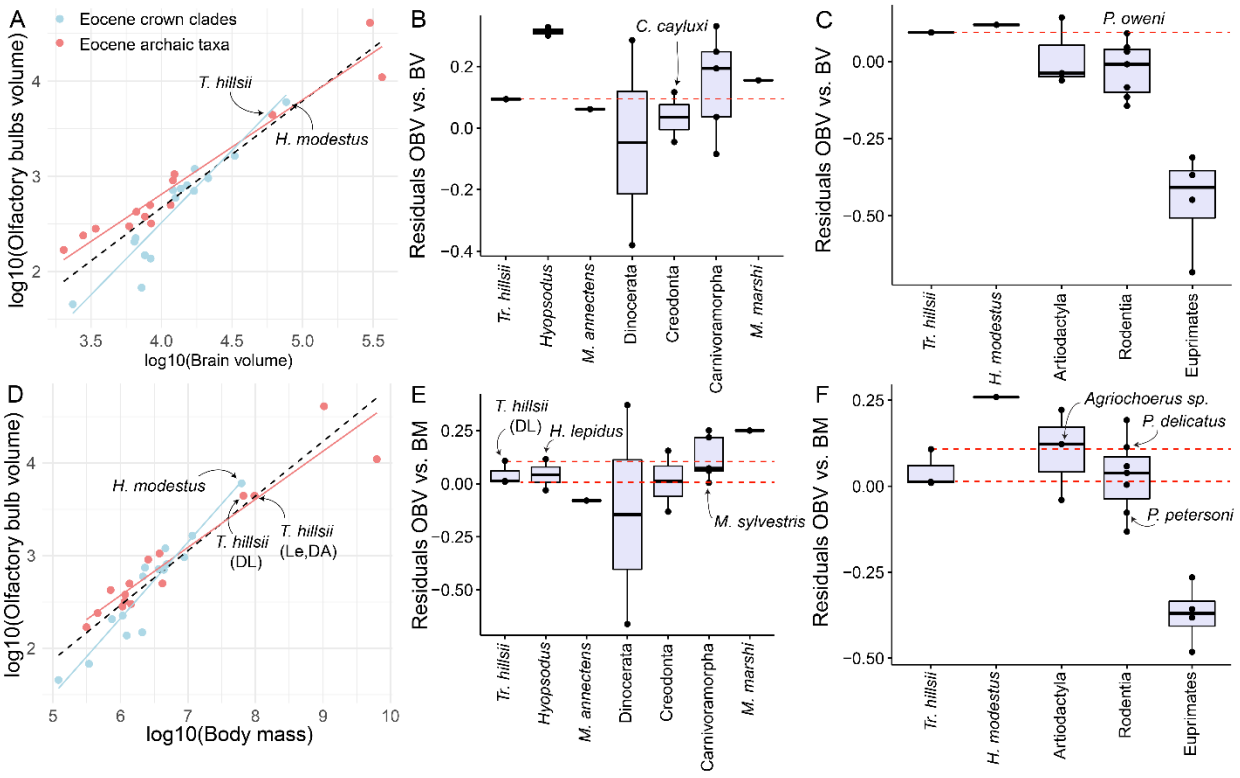

Figure 8. Relative and absolute size of the olfactory bulbs of middle Eocene mammals. A. Linear regression of log10 (Olfactory bulb volume area vs. Endocranial volume) for archaic groups and crown clades, B. Boxplot of the residuals from the equation in A. for *Trogosus* and other archaic groups, C. Boxplot of the residuals from the equation in A. for *Trogosus* and crown clades. D. Linear regression of log10 (Olfactory bulb volume area vs. Body mass) for archaic groups and crown clades, E. Boxplot of the residuals from the equation in D. for *Trogosus* and other archaic groups, F. Boxplot of the residuals from the equation in D. for *Trogosus* and crown clades. See table S2 for residual values. Volumetric measurements are in cubic millimeters and body mass was measured in milligrams. **Abbreviations:** BM, body mass; BV, brain volume; OBV, olfactory bulb volume.

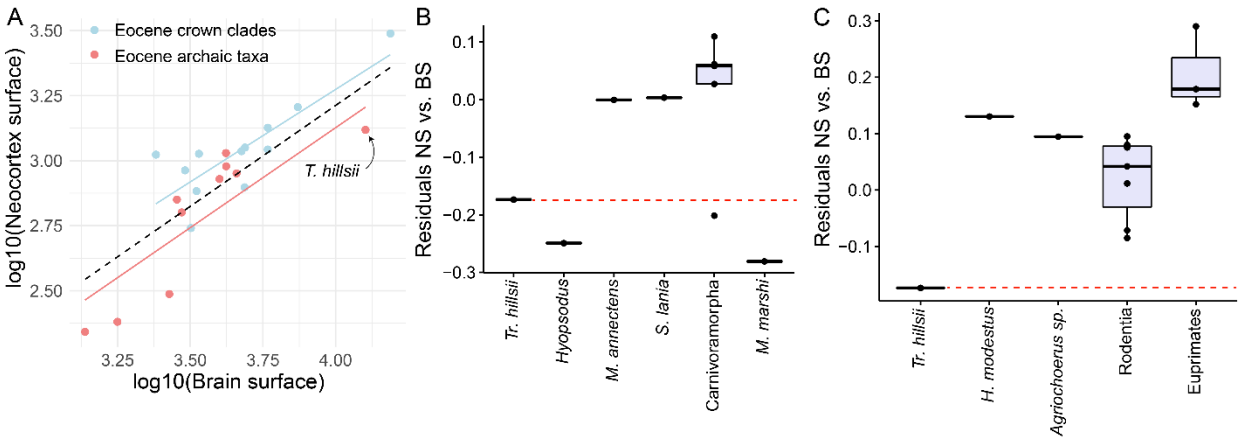

1

2 **Figure 9.** Relative size of the neocortex of middle Eocene mammals. A. Linear regression of
3 log10 (Neocortical surface area vs. Endocranial surface area) for archaic groups and crown
4 clades, B. Boxplot of the residuals from the equation in A. for *Trogosus* and other archaic
5 groups, C. Boxplot of the residuals from the equation in A. for *Trogosus* and crown clades. See
6 table S2 for residual values. Surface area measurements are in square millimeters.
7 **Abbreviations:** BS, brain surface; NS, neocortical surface.

8

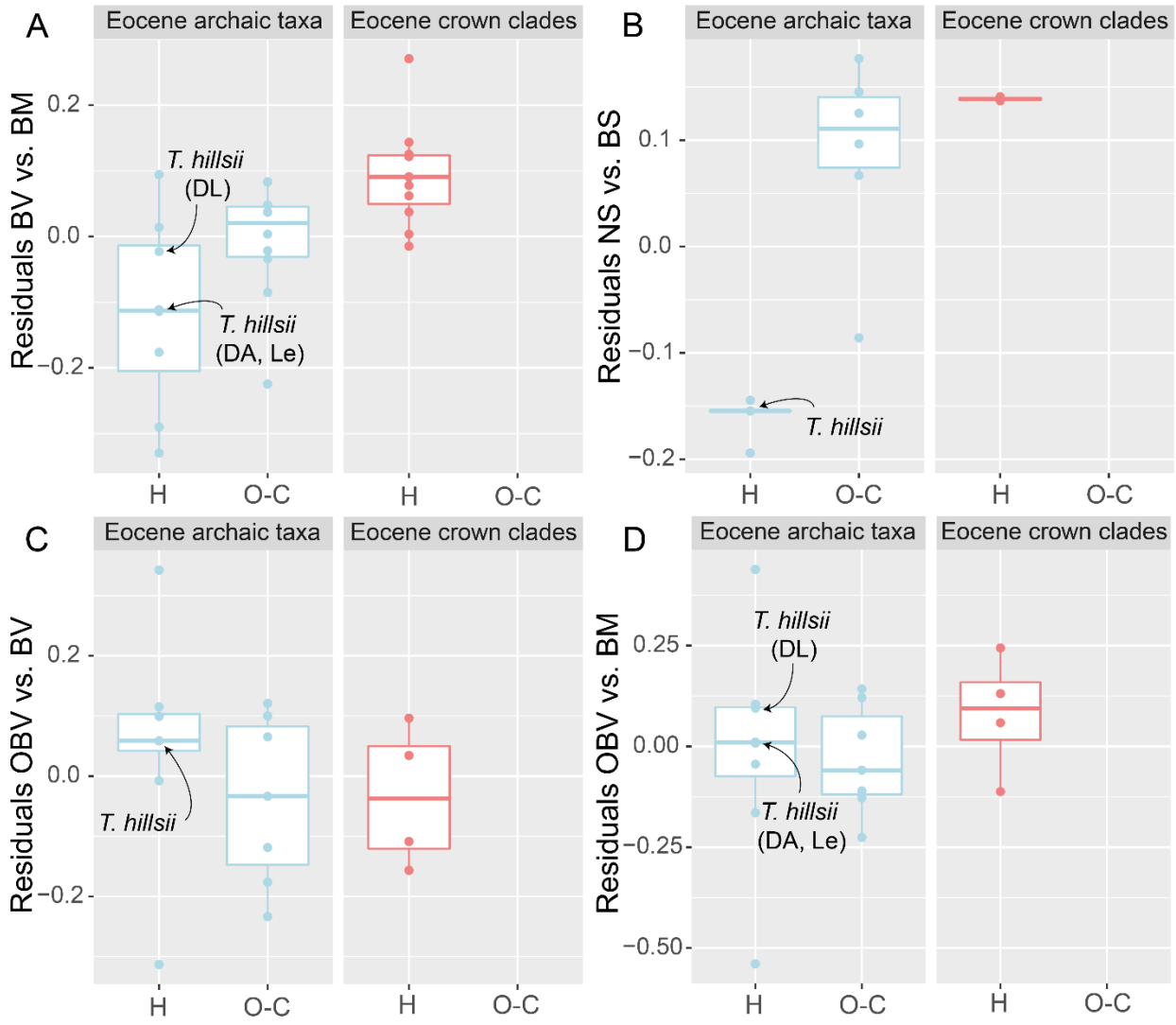

Figure 10. Relative size of the brain, neocortex, olfactory bulbs and absolute size of the olfactory bulbs organized by dietary guilds and grade. A. Boxplot of the residuals log10 (Endocranial volume area vs. Body mass), B. Boxplot of the residuals log10 (Neocortical surface area vs. Endocranial surface area), C. Boxplot of the residuals log10 (Olfactory bulb volume area vs. Endocranial volume) D. Boxplot of the residuals log10 (Olfactory bulb volume area vs. Body mass). See table S3 for residual values. **Abbreviations:** BM, body mass; BV, brain volume; OBV, olfactory bulb volume; BS, brain surface; H, herbivorous mammals; NS, neocortical surface; O-C, omnivorous-carnivorous mammals.

Supporting Information

Figure S1. Cranium of *Trogosus hillsii* (USNM 17157). A. lateral view of the cranium. B. CT cross-sectional view of the braincase. The line in A denotes the plane of the cross-sectional view (Slice 758).

Table S1. Endocranial volumes and surface areas data gathered for our sample. Body mass, endocranial, olfactory bulb volume, endocranial and neocortical surface areas for the specimens used in the different analyses. Data are from Bertrand et al. (2022).

Table S2. Results from the OLS regressions for the different endocranial variables and for archaic taxa, crown clades, and all taxa. Abbreviations: BM, Body mass; BR, brain volume; BS, Brain surface; Df, degrees of freedom; Neo, Neocortex surface; OB, olfactory bulb volume; RSE, Residual standard error. The p-value predictor corresponds to body mass (1, 3), brain volume (2), and brain surface (4). Group = archaic taxa and crown clades.

Table S3. Residuals of the endocranial volume vs. body mass, olfactory bulb volume vs. endocranial volume, olfactory bulb volume vs. body mass and neocortical surface area vs. endocranial surface area. Values used to make boxplots in figures 7, 8, and 9. Note, the EQ values were not plotted. Abbreviations: BM, Body mass; BR, brain volume; BS, Brain surface; EQ, Encephalization quotient; Neo, Neocortex surface; OB, olfactory bulb volume.

Table S4. Asymptotic K-Sample Fisher-Pitman Permutation Test, Welch test, and pairwise comparisons for Eocene archaic taxa and crown clades. Significant adjusted p-values are in bold. Abbreviations: BM, body mass; BR, brain volume; BS, Brain surface; df, degrees of freedom; Neo, Neocortex surface; OB, olfactory bulb volume (See figures 7, 8, and 9).

Table S5. Results from the non-phylogenetic corrected ANOVA using Residual Randomization. Abbreviations: BM, Body mass; BR, brain volume; BS, Brain surface; Df, degrees of freedom; MS, Mean squares; Neo, Neocortex surface; OB, olfactory bulb volume; SS, Sum of squares; R2, coefficient of determination. Group = archaic taxa and crown clades.

Table S6. Residuals of the endocranial volume vs. body mass, olfactory bulb volume vs. endocranial volume, olfactory bulb volume vs. body mass and neocortical surface area vs. endocranial surface area for dietary groups only. Values used to make boxplots in figure 10. Note, the EQ values were not plotted. Abbreviations: BM, Body mass; BR, brain volume; BS, Brain surface; EQ, Encephalization quotient; Neo, Neocortex surface; OB, olfactory bulb volume.

Table S7. Asymptotic K-Sample Fisher-Pitman Permutation Test, Welch test, and pairwise comparisons for the two dietary groupings. Significant adjusted p-values are in bold. Abbreviations: BM, body mass; BR, brain volume; BS, Brain surface; df, degrees of freedom; Neo, Neocortex surface; OB, olfactory bulb volume (See figure 10).